HHS Public Access

Author manuscript

Cell Rep. Author manuscript; available in PMC 2019 December 06.

Published in final edited form as:

Cell Rep. 2019 November 12; 29(7): 1848–1861.e6. doi:10.1016/j.celrep.2019.10.012.

Control of Germinal Center Localization and Lineage Stability of Follicular Regulatory T Cells by the Blimp1 Transcription Factor

Erxia Shen[1,2,3,11], **Hardis Rabe**[1,2,6,11], **Lin Luo**[4,5,11], **Lei Wang**[1,2,11], **Qin Wang**[1,2,7], **Jie Yin**[4,8], **Xueying Yang**[1,2], **Wenquan Liu**[1,2,9], **Jessica M. Sido**[1,2], **Hidetoshi Nakagawa**[1,2], **Lin Ao**[1,2], **Hye-Jung Kim**[1,2,12], **Harvey Cantor**[1,2,12,13,*], **Jianmei W. Leavenworth**[4,10,12,*]

[1]Department of Cancer Immunology and Virology, Dana-Farber Cancer Institute, Boston, MA 02115, USA

[2]Department of Immunology, Harvard Medical School, Boston, MA 02115, USA

[3]Department of Pathogenic Biology and Immunology, Guangzhou Hoffmann Institute of Immunology, School of Basic Sciences, Guangzhou Medical University, Guangzhou 510182, China

[4]Department of Neurosurgery, University of Alabama at Birmingham, Birmingham, AL 35233, USA

[5]School of Pharmacy and Jiangsu Province Key Laboratory for Inflammation and Molecular Drug Target, Nantong University, Nantong, Jiangsu 226001, China

[6]Department of Infectious Diseases, Institute of Biomedicine, Sahlgrenska Academy, University of Gothenburg, Göteborg, Sweden

[7]Department of Immunology, Medical College of Soochow University, Suzhou, Jiangsu 215123, China

[8]Department of Cell Biology, Tianjin Medical University, Tianjin 300070, China

[9]Department of Parasitology, Wenzhou Medical University, Wenzhou, Zhejiang 325035, China

[10]Department of Microbiology, University of Alabama at Birmingham, Birmingham, AL 35233, USA

[11]These authors contributed equally

[12]Senior author

[*]Correspondence: harvey_cantor@dfci.harvard.edu (H.C.), jleavenworth@uabmc.edu (J.W.L.).

AUTHOR CONTRIBUTIONS

J.W.L., L.W., E.S., L.L., and H.R. designed and performed the experiments, analyzed the data, and interpreted the results. Q.W., W.L., and X.Y. assisted with the flow cytometry analysis, immunoblot and qRT-PCR, and retroviral infection and ELISA assays. J.W.L., L.L., and J.Y. performed the lentiviral infection and ChIP-PCR experiments. X.Y. performed the confocal microscopy analysis. J.M.S., H.N., and L.A. assisted with the adoptive transfer and flow cytometry analysis of the pSTAT3 and pSTA5 levels. J.W.L., L.W., E.S., H.R., H.-J.K., and H.C. wrote the paper. J.W.L. and H.C. conceived and supervised the study.

DECLARATION OF INTERESTS

The authors declare no competing interests.

SUPPLEMENTAL INFORMATION

Supplemental Information can be found online at https://doi.org/10.1016/j.celrep.2019.10.012.

[13]Lead Contact

SUMMARY

Follicular regulatory T (T_{FR}) cells are a specialized suppressive subset that controls the germinal center (GC) response and maintains humoral self-tolerance. The mechanisms that maintain T_{FR} lineage identity and suppressive activity remain largely unknown. Here, we show that expression of Blimp1 by FoxP3$^+$ T_{FR} cells is essential for T_{FR} lineage stability, entry into the GC, and expression of regulatory activity. Deletion of Blimp1 in T_{FR} cells reduced FoxP3 and CTLA-4 expression and increased pro-inflammatory cytokines and spontaneous production of autoantibodies, including elevated IgE. Maintenance of T_{FR} stability reflected Blimp1-dependent repression of the IL-23R-STAT3 axis and activation of the CD25-STAT5 pathway, while silenced IL-23R-STAT3 or increased STAT5 activation rescued the Blimp1-deficient T_{FR} phenotype. Blimp1-dependent control of CXCR5/CCR7 expression also regulated T_{FR} homing into the GC. These findings uncover a Blimp1-dependent T_{FR} checkpoint that enforces suppressive activity and acts as a gatekeeper of GC entry.

In Brief

Wang et al. identify Blimp1 as a critical transcription factor for the proper positioning and stable expression of the suppressive activity of T_{FR} cells that control GC responses. In the absence of Blimp1, unstable T_{FR} cells prematurely migrate into the GC and differentiate into T_{FH}-like cells to promote dysregulated GC responses.

Graphical Abstract

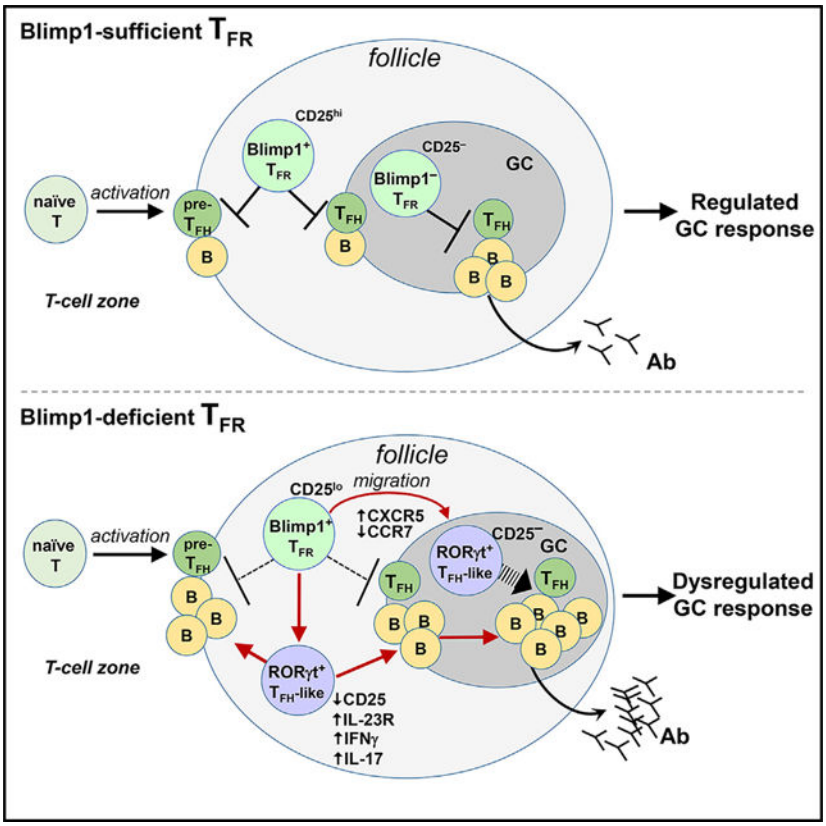

INTRODUCTION

Germinal centers (GCs) are specialized dynamic structures that provide a unique niche for B cells to generate high-affinity antibody (Ab) responses to microbial pathogens after infection or vaccination. The GC response takes place in the context of substantial cell death and apoptosis, which provides a potential arsenal of self-antigens that may activate autoreactive Ab responses. Under these circumstances, the induction of cognate GC B cells by follicular helper T cells (T_{FH}) may result in excessive Ab responses that include autoantibodies to self-tissues (Crotty, 2011, 2014). Since dysregulated GC responses may be at the root of an array of systemic autoimmune diseases (Crotty, 2011, 2014; Leavenworth et al., 2013, 2015), insight into mechanisms that control these responses is essential.

There is abundant evidence that immune responses and self-tolerance are stringently controlled by FoxP3$^+$ regulatory T cells (Treg). FoxP3$^+$ Treg are composed of a central Treg (cTreg) component and several tissue-specific sublineages of effector Treg (eTreg), including the recently defined subset of follicular regulatory T cells (T_{FR}) that regulate GC responses through interactions with activated T_{FH} and GC B cells (Chung et al., 2011; Leavenworth et al., 2015; Linterman et al., 2011; Sage and Sharpe, 2015; Smigiel et al., 2014). T_{FR} cells share several features with T_{FH} cells, including the expression of ICOS, PD-1, and CXCR5 receptors that contribute to T_{FR} differentiation and follicular localization (Chung et al., 2011; Linterman et al., 2011; Wing et al., 2017). T_{FR} cells also co-opt the expression of Bcl6, the cardinal transcription factor (TF) that guides follicular CD4$^+$ T cell

differentiation (Chung et al., 2011; Leavenworth et al., 2015; Linterman et al., 2011). The differentiation of Treg precursors into T_{FR} cells is associated with signs of cellular activation and the upregulation of genes expressed by eTreg, including GITR, CTLA-4, ICOS, KLRG1, and the Blimp1 TF (Linterman et al., 2011). Although it is likely that strong T cell receptor (TCR) signals favor T_{FR} cell differentiation (Kallies et al., 2006; Linterman et al., 2011), the mechanisms that ensure the maintenance of lineage identity and expression of regulatory activity by T_{FR} are not well defined.

T_{FR} cells, like other eTreg, express the Blimp1 TF (Cretney et al., 2011; Linterman et al., 2011; Vasanthakumar et al., 2015). Recent analyses suggest that Blimp1 may not make a significant contribution to T_{FR} differentiation and may even have a negative impact on the T_{FR} response. This view is supported by findings that Blimp1 expression may reduce T_{FR} expansion and development (Botta et al., 2017; Linterman et al., 2011), and that the downregulation of Blimp1 expression is associated with the acquisition of T_{FR} effector activity and navigation into the GC (Wing et al., 2017).

Here, we report that Blimp1 expression is essential to maintain T_{FR} lineage stability, appropriate positioning in the GC, and effective regulatory activity. Blimp1 regulates CTLA-4 expression and signals transmitted by interleukin (IL)-23R and CD25 to maintain the T_{FR} phenotype. The upregulation of IL-23R by Blimp1-deficient T_{FR} resulted in enhanced STAT3 signaling, diminished FoxP3 expression, and impaired regulatory activity. Blimp1-deficient T_{FR} cells displayed reduced CTLA-4 expression and acquired an effector T cell phenotype and expression of IL-4, which was accompanied by high levels of immunoglobulin E (IgE) and serum autoantibodies. Blimp1-dependent control of the CXCR5-CCR7 axis was also essential for the correct positioning of T_{FR} within the GC. These findings suggest that the expression of Blimp1 in T_{FR} is essential for differentiation into functional T_{FR} with a stable phenotype.

RESULTS

FoxP3-Specific Deletion of Blimp1 Leads to Dysregulated GC Responses

To investigate the contribution of Blimp1 to the differentiation and regulatory function of $FoxP3^+$ T_{FR}, we generated mice in which *Prdm1* alleles were deleted in *FoxP3*$^+$ T cells (*Prdm1*$^{fl/fl}$*FoxP3*^{Cre} mice) and confirmed Blimp1 deficiency in T_{FR} cells (Figures S1A and S1B). We noted a 3-fold increase in the GC area at 4–5 months of age, a 6- to 8-fold increase in the frequency of T_{FH} cells ($CD4^+CD3^+ICOS^{hi}CXCR5^+FoxP3^-$), and a 5- to 10-fold increase in $B220^+GL\text{-}7^+Fas^+$GC B cells compared with *FoxP3*^{Cre} (wild-type [WT]) controls (Figures 1A and 1B). This T_{FH}-GC expansion was associated with high titers of anti-nuclear autoantibodies (ANAs) and IgE levels beginning at 1.5 months and increasing with age (Figure 1C). We also observed an increased frequency and number of T_{FH} and GC B cells and ($CD4^+FoxP3^-CD44^{hi}CD62L^{lo}$) effector T cells in *Prdm1*$^{fl/fl}$*FoxP3*^{Cre} (knockout [KO]) mice compared with WT controls in the steady state at an early age (6 weeks old) (Figures 1D, 1E, and S1C).

Blimp1 is expressed by eTreg subsets located in both lymphoid and non-lymphoid tissues (e.g., intestine, skin, fat, possibly lung), and may be essential for IL-10 production (Cretney

et al., 2013). However, examination of non-lymphoid tissues (skin, adipose tissue, lung) from 4– 5-month-old *Prdm1*$^{fl/fl}$ *FoxP3*^{Cre} mice failed to detect histological abnormalities, with the exception of mild to moderate inflammation in the colon (Figure S1D), which is consistent with diminished eTreg IL-10 production, as noted by others (Cretney et al., 2011; Kallies et al., 2006; Martins et al., 2006). In view of a recent study that IL-10 production by T_{FR} cells promotes the GC response (Laidlaw et al., 2017), the above findings, along with the observations of increased numbers and sizes of GCs, suggested that the primary contribution of Blimp1 expression by Treg may entail an IL-10-independent regulation of humoral self-tolerance, perhaps by FoxP3$^+$ T_{FR} cells.

Prdm1$^{fl/fl}$*FoxP3*^{Cre} Mice Develop Dysregulated GC Responses after Antigen Challenge

To understand the contribution of Blimp1 to Treg-mediated control of Ab responses, we analyzed antigen-specific GC responses after immunizing 6-week-old mice with the hapten NP coupled to KLH (NP-KLH). One week after immunization, *Prdm1*$^{fl/fl}$*FoxP3*^{Cre} mice displayed increased T_{FH} and GC B cells along with CD4$^+$ effector T cells (Figures 1F, 1G, and S1C) and markedly increased (>20-fold) anti-NP IgG titers (Figure 1H) compared to WT mice. The partial loss of Blimp1 expression in heterozygous *Prdm1*$^{fl/+}$*FoxP3*^{Cre} mice also resulted in increased numbers of T_{FH} and GC B cells (Figures 1F and 1G) and elevated anti-NP titers after immunization (Figure 1H). The increased frequency of T_{FH} and GC B cells that is apparent at 3 weeks after the primary immune response persisted 7 days after the secondary challenge (Figure S1E). Given the critical role of IL-21 and IL-4 cytokine-producing T_{FH} in inducing IgE and IgG1 responses (Harada et al., 2012), we determined the numbers of IL-21/IL-4-producing T_{FH} after immunization (Weinstein et al., 2016) and observed a significant increase in both the numbers of T_{FH} and cytokine-producing T_{FH} cells in KO mice at day 7 after immunization (Figure S1F). Thus, expression of Blimp1 by FoxP3$^+$ T cells may be required to suppress the GC response, including “natural” IgE levels and Abs produced after immunization with foreign antigen.

Abnormal Treg and T_{FR} Cell Homeostasis in *Prdm1*$^{fl/fl}$*FoxP3*^{Cre} Mice

In view of the robust GC responses of *Prdm1*$^{fl/fl}$*FoxP3*^{Cre} mice, we were surprised to note the increased numbers of FoxP3$^+$ Treg in the steady state and after immunization (Figures 2A, 2B, and S2A), as well as in the 4- to 5-month-old mice (Figures S2B and S2C). Analysis of mixed bone marrow chimeras, generated by the reconstitution of *Rag2*$^{-/-}$ hosts with CD45.2$^+$Prdm1$^{fl/fl}$FoxP3^{Cre} and B6.CD45.1$^+$ bone marrow cells, and as a control, a mixture of WT and B6.CD45.1$^+$ cells, revealed that Blimp1 deficiency within the FoxP3$^+$ lineage mainly affected eTreg but not cTreg (Figure S2D). We then analyzed eTreg subsets, T_{FR} (CD4$^+$CD3$^+$PD-1$^+$CXCR5$^+$FoxP3$^+$) and non-T_{FR} (CD4$^+$CD3$^+$CXCR5$^-$FoxP3$^+$) cells. For unimmunized 7- to 9-week-old mice, although Blimp1 deficiency resulted in increased FoxP3$^+$ T_{FR} and non-T_{FR} cells, the 14.5-fold T_{FR} increase compared to that in WT mice was substantially greater than the 1.2-fold increase noted for total Treg and non-T_{FR} Treg (1.8-fold) (Figure S2A). An analysis of 4- to 5-month-old unimmunized mice also showed that the numbers of Blimp1 KO T_{FR} were dramatically increased compared to WT T_{FR} (~8- to 10-fold in the spleen and mesenteric lymph node [mLN]), while the numbers of total Blimp1-deficient Treg were only slightly increased compared to WT Treg, with the exception of a significant increase in Blimp1-deficient non-T_{FR} in mLNs (~4-fold) (Figures

S2B and S2C). Immunization with 4-hydroxy-3-nitrophenylacetyl-ovalbumin (NP-OVA) also resulted in the substantial expansion of T_{FR} cells from *Prdm1*$^{fl/fl}$*FoxP3*^{Cre} mice compared to WT mice, while the expansion of non-T_{FR} was modest in comparison (Figures 2A and 2B). Although FoxP3$^+$ Treg and T_{FR} cells from *Prdm1*$^{fl/fl}$*FoxP3*^{Cre} mice expressed similar levels of Bcl2 (Figure S2E), they displayed increased Ki67 expression and diminished levels of annexin V, indicating a relatively high rate of proliferation and reduced apoptosis (Figure 2C). The heightened T_{FR} proliferative response was apparently uncoupled to T_{FR} activation, as judged by reduced expression of the CD69 marker of T_{FR} (but not CXCR5$^-$ Treg) (Figure 2C). These results suggested that Blimp1 may normally limit the survival and expansion of FoxP3$^+$ eTreg cells *in vivo*.

Impaired Suppressive Phenotype of Treg and T_{FR} Cells in *Prdm1*$^{fl/fl}$*FoxP3*^{Cre} Mice

Examination of expanded FoxP3$^+$ T_{FR} and non-T_{FR} conventional Treg in the spleen of unimmunized and immunized young *Prdm1*$^{fl/fl}$*FoxP3*^{Cre} mice revealed reduced expression of FoxP3 and other Treg-associated molecules, including CTLA-4, compared to cells from WT mice (Figures 2D and S2F), suggesting a functionally impaired phenotype (Wing et al., 2014). We also noted that T_{FR} cells but not non-T_{FR} cells from unimmunized *Prdm1*$^{fl/fl}$*FoxP3*^{Cre} mice produced substantially higher levels of interferon γ (IFNγ) compared to WT cells (Figure S2G). Moreover, T_{FR} cells from immunized *Prdm1*$^{fl/fl}$*FoxP3*^{Cre} mice produced increased IL-17A, IFNγ, and IL-4 pro-inflammatory cytokines (Figure 2E). These results suggested that Blimp1 deficiency resulted in the expansion of FoxP3^{lo} Treg, particularly FoxP3^{lo} T_{FR}, that expressed reduced levels of Treg-associated receptors and increased levels of effector cytokines.

The expression of CD25 on T_{FR} cells is downregulated as they mature and migrate into the GC, and these highly differentiated CD25$^{lo/-}$ T_{FR} cells express low but significant levels of Blimp1 compared to their naive Treg precursors (Wing et al., 2017). Our finding that T_{FR} cells from *Prdm1*$^{fl/fl}$*FoxP3*^{Cre} mice displayed reduced CD25 expression (Figure 2D) prompted us to fully define the impact of Blimp1 deficiency on T_{FR} cells that expressed progressively diminishing levels of CD25 (Figure S2H). Although all Blimp1-deficient CD25-expressing T_{FR} expressed reduced levels of FoxP3 and CTLA-4, the highest level of FoxP3 was expressed by the CD25^{hi} T_{FR} subset (Figure 2F), suggesting that Blimp1 deficiency resulted in the expansion of T_{FR} cells with an impaired suppressive phenotype, including a mature “GC” CD25^{lo} T_{FR} subset.

To examine the phenotype of Blimp1-deficient T_{FR} cells under more physiological conditions, we analyzed female heterozygous *Prdm1*$^{fl/fl}$*FoxP3*$^{Cre/+}$ mice. Due to the X-linked nature of the *FoxP3*^{Cre} knockin transgene, these mice have both YFP$^+$ Blimp1-deficient Treg and YFP$^-$ Blimp1-sufficient Treg. A comparison of the phenotype of YFP$^+$ and YFP$^-$ T_{FR} cells revealed that YFP$^+$ Blimp1-deficient T_{FR} cells express reduced levels of FoxP3, CTLA-4, and GITR, as well as increased levels of RORγt and IL-17A at day 10 after NP-OVA immunization (Figure 2G). These findings indicate that Blimp1-deficient T_{FR} display an impaired suppressive phenotype and upregulated inflammatory cytokine production in a relatively non-inflammatory setting.

Altered GC Distribution of T_{FR} Cells in *Prdm1*$^{fl/fl}$*FoxP3*^{Cre} Mice

Further analysis of T_{FR}-specific gene expression revealed that T_{FR} cells from *Prdm1*$^{fl/fl}$*FoxP3*^{Cre} mice expressed elevated levels of Bcl6 and CXCR5 (Figures 2D and 2H) (Linterman et al., 2011). The upregulation of CXCR5 along with diminished CCR7 expression in follicular T cells may be essential for navigation from the T cell zone into the GC (Crotty, 2011; Wing et al., 2017). *Prdm1*$^{fl/fl}$*FoxP3*^{Cre} mice had fewer CCR7^{+} T_{FR} and, in general, lower CCR7 levels compared to WT T_{FR} (Figures 2I and S2I). Confocal analysis revealed a higher number of T_{FR} and T_{FH} cells within the GC of *Prdm1*$^{fl/fl}$*FoxP3*^{Cre} mice compared to WT mice 2 weeks after NP-OVA immunization (Figure 2J). These results suggested that FoxP3-specific deletion of Blimp1 resulted in an enrichment of T_{FR} cells in the GC that express a functionally impaired phenotype.

FoxP3-Specific Ablation of Blimp1 Impairs T_{FR} Suppressive Activity after Adoptive Transfer

To determine whether Blimp1-deficient conventional (non-T_{FR}) Treg may contribute to dysregulated GC responses, we compared *Bcl6*$^{fl/fl}$*Prdm1*$^{fl/fl}$*FoxP3*^{Cre} to *Bcl6*$^{fl/fl}$*FoxP3*^{Cre} mice that do not contain T_{FR} cells (Figures 3A and 3B). While the latter strain contains an intact (Blimp1-sufficient) conventional Treg population, the former strain harbors only Blimp1-deficient Treg (Figures 3A and 3B). The frequency of T_{FH}, GC B cells, and serum Ab titers were substantially reduced in *Bcl6*$^{fl/fl}$*Prdm1*$^{fl/fl}$*FoxP3*^{Cre} mice (to levels similar to *Bcl6*$^{fl/fl}$ *FoxP3*^{Cre} and WT mice) compared with *Prdm1*$^{fl/fl}$*FoxP3*^{Cre} mice (Figures 3A and 3B), indicating that Blimp1-deficient conventional Treg do not contribute significantly to the increased frequency of T_{FH} and GC B cells or the dysregulated Ab responses observed in *Prdm1*$^{fl/fl}$*FoxP3*^{Cre} mice.

Analysis of purified T_{FR} cells from *Prdm1*$^{fl/fl}$*FoxP3*^{Cre} mice indicated that they failed to inhibit *in vitro* IgG production by mixtures of T_{FH} and B cells compared to WT counterparts (Figures S2J and S2K). We then transferred purified T_{FR} from CD45.2^{+} Blimp1-deficient or WT donors along with CD45.1^{+} T_{FH} and B cells from NP-OVA-immunized mice into *Rag2*$^{-/-}$ hosts and challenged with NP-OVA (Figures 3C and S2L). After the transfer, T_{FR} cells included a subpopulation of ex-T_{FR} cells that were PD-1^{-}CXCR5^{-}, reflecting the dynamic state of T_{FR} differentiation during the GC response (Wing et al., 2017) (Figure 3D). Transferred Blimp1-deficient T_{FR} expressed increased levels of IFN-γ and IL-17A (Figure 3E), reduced levels of FoxP3, CD25, CTLA-4, and GITR (Figure 3F), and demonstrated impaired regulatory activity, as judged by increased numbers of T_{FH} and GC B cells (Figure 3G), heightened IgG, IgG1, and IgE anti-NP responses, and elevated ANAs (Figure 3H). These changes resulted solely from the differences in Blimp1 expression in T_{FR} cells, indicating that Blimp1 expression is essential for the suppressive activity expressed by isolated T_{FR}.

Tamoxifen-Induced Blimp1 Deletion Impairs Lineage Stability and Functional T_{FR} Differentiation

To define the precise stage at which Blimp1 affects T_{FR} differentiation, we used an inducible Blimp1 deletion system to circumvent potential developmental defects secondary to inflammatory or other changes in the environment. We generated *Prdm1*$^{fl/fl}$*iCre*$^{+}$ or

Prdm1$^{fl/fl}$*iCre*$^{-}$ mice after crossing *Prdm1*$^{fl/fl}$ mice with Rosa26-$^{Cre\text{-}ERT2}$ (referred to as iCre) transgenic mice to allow the conditional deletion of Blimp1 after the administration of tamoxifen. We treated *Prdm1*$^{fl/fl}$iCre^{+} mice and *Prdm1*$^{fl/fl}$*iCre*$^{-}$ control mice with tamoxifen 1 day before isolation of CD25^{hi} Treg and co-transferred these cells along with naive CD4^{+} T cells into *Tcra*$^{-/-}$ hosts, followed by immunization with NP-OVA and injection of tamoxifen into these hosts for 3 more days (Figure S3A). Acute reduction of Blimp1 in Treg immediately before immunization resulted in increased numbers of T_{FR} and CD138^{+} plasma cells in adoptive hosts (Figures S3B and S3C).

To determine whether continued Blimp1 expression was required for suppressive activity in differentiated T_{FR} in the absence of other FoxP3^{+} eTreg, we isolated CD4+PD-1^{+}CXCR5^{+}GITR^{+} T_{FR} cells (CD45.2^{+}) from *Prdm1*$^{fl/fl}$iCre^{+} mice or *Prdm1*$^{fl/fl}$*Cre*$^{-}$ control mice 6 days after NP-OVA immunization and 1 day after tamoxifen administration. We transferred these cells along with T_{FH} cells from immunized CD45.1^{+} mice into *Tcra*$^{-/-}$ hosts before challenge with NP-OVA and injection of tamoxifen for 3 more days (Figure 4A). We observed substantially reduced Blimp1 and increased Bcl6 expression by T_{FR} cells from *Prdm1*$^{fl/fl}$iCre^{+} mice (Figure 4B), along with an increased frequency of T_{FR}, T_{FH}, and GC B cells (Figure 4C). Defective suppressive activity of FoxP3^{lo} T_{FR} after acute Blimp1 depletion was accompanied by increased production of pro-inflammatory IL-17A and IFNγ cytokines (Figures 4D and 4E), suggesting that acute deletion of Blimp1 led to the differentiation of T_{FR} into TH effector-like cells. T_H1/T_H17-like conversion was not apparent in Blimp1-deleted ex-T_{FR} cells (PD1^{-}CXCR5^{-}) (Figures 4D and 4E). These results suggested that transferred Blimp1-deleted and control T_{FR} cells both contained "ex-T_{FR}" cells that had lost the T_{FR} phenotype, but only the Blimp1-deleted T_{FR} population displayed functional instability that may provide the *de novo* helper function for B cells that promote dysregulated GC and Ab responses.

Blimp1-Deficient T_{FR} but Not Conventional Treg Display Lineage Instability and Conversion into T_{FH}-like Cells

To further test the above proposition, we transferred T_{FR} or non-T_{FR} cells from *Prdm1*$^{fl/fl}$*FoxP3*^{Cre} mice or WT mice separately into *Tcra*$^{-/-}$ hosts followed by analysis of T_{FR} and T_{FH} cells and the Ab response after NP-OVA immunization (Figure 4F). The results showed that mice transferred with Blimp1-deficient T_{FR} cells had the highest Ab titers associated with the highest frequencies of T_{FH} compared to the other groups that had similar levels of T_{FH} cells Ab titers. Although both Blimp1-deficient T_{FR} and non-T_{FR} cells expressed the pro-inflammatory cytokine IL-17A, the former had the largest portion that converted into T_H17-like cells (Figure 4F). These findings indicate that Blimp1-deficient T_{FR} but not conventional Treg acquired T_H activity, showed impaired suppressive activity and contributed to the dysregulated GC responses, and that continued Blimp1 expression by T_{FR} is required for the maintenance of T_{FR} functional stability.

Mechanism of Blimp1-Dependent Regulation of the T_{FR} Suppressive Phenotype and Lineage Stability

Comparison of the transcriptional profiles of WT and *Prdm1*$^{fl/fl}$*FoxP3*^{Cre} T_{FR} cells (Figure 5A) revealed that ~460 genes were upregulated and 300 genes were downregulated in

Blimp1-deficient T_{FR} cells. Ingenuity pathway analysis of differentially (1.5-fold cutoff) expressed genes showed that Blimp1 deficiency affected pathways associated with cytokine signaling and T_H cell differentiation (Figure S4A). Genes that regulate the differentiation of T_H2 cells (*Il4*), T_H17 cells *(Il23r),* and T_{FH} cells *(Cxcr5, Bcl6, Il21)* were strongly upregulated, while genes associated with suppressive activity *(Il10, Il2ra, GzmB)* were downregulated (Figure 5B), suggesting that diminished suppressive activity of Blimp1-deficient T_{FR} cells may be associated with conversion to T effector cells.

Blimp1 Represses IL-23R-STAT3 Signaling and CXCR5 Expression but Retains CD25-STAT5 Activation in Differentiating T_{FR} Cells

Gene Ontology (GO) analysis indicated that the gene groups upregulated in Blimp1-deficient T_{FR} included genes that regulated cytokine-cytokine receptor interactions (Figures 5C, S4B, and S4C), and that the *Il23r* gene was one of the most upregulated genes in Blimp1-deficient T_{FR} (Figures 5B and 5C). T_{FR} cells after tamoxifen-induced Blimp1 depletion confirmed the increased expression of IL-23R by Blimp1-deleted T_{FR} cells (Figure 5D). T_{FR} cells from *Prdm1*$^{fl/fl}$*FoxP3*^{Cre} mice, including the mature "GC" CD25^{lQ} subset, expressed higher levels of IL-23R than T_{FR} cells from WT mice (Figure 5E). Consistent with expression at the protein levels (Figures 2D and 2H), Blimp1-deficient T_{FR} also expressed elevated *Cxcr5* and reduced *Il2ra* and *Ccr7* at the RNA levels (Figures 5B and 5C). These results suggested that Blimp1 may downregulate IL-23R and CXCR5 expression but positively regulate CD25 and CCR7 expression by T_{FR} cells.

To define Blimp1-dependent regulation of the *Il23r*, *Il2ra*, *Cxcr5*, and *Ccr7* genes, we analyzed the interaction of Blimp1 with these gene loci according to chromatin immunoprecipitation (ChIP)-PCR. Blimp1 bound to the 3rd intron of the *Il23r* gene and the 1st intron of the *Cxcr5* gene in Treg, but not naive CD4$^+$ T cells isolated from immunized mice (Figure 5F). These interactions were associated with the presence of repressive chromatin H3K27me3 but not acetylated histone H3 (AcH3) marks (Figure 5F). Blimp1 also bound to the 1st intron of *Il2ra* and the 3rd intron of *Ccr7* as well as the 5′ distal element of the *CTLA-4* gene, which contained AcH3 activation marks (but not H3K27me3 repressive marks) (Figure 5F). Blimp1 did not bind to the *FoxP3* gene, suggesting that Blimp1 does not directly regulate FoxP3 expression (Figure 5F) (Garg et al., 2019). Thus, Blimp1 may repress the transcription of the *Il23r* and *Cxcr5* genes but activate the transcription of the *Il2ra*, Ccr7, and *CTLA-4* genes in Treg, which is consistent with the view that Blimp1 can function as both a transcriptional activator and a repressor (Minnich et al., 2016).

The ability of FoxP3$^+$ Treg to maintain high levels of FoxP3 expression and lineage stability in the face of intense inflammatory responses depends in part on robust CD25-STAT5 activation and binding of activated STAT5 to the *FoxP3 CNS2* intronic element (Feng et al., 2014; Kim et al., 2015). In contrast, the engagement of IL-23R promotes STAT3 activation to promote Treg conversion into T_H17-like cells (Laurence et al., 2012). We tested the premise that Blimp1 may modulate the balance between IL-23R-STAT3 and CD25-STAT5 signals in T_{FR} in favor of the latter. Analysis of tamoxifen-induced Blimp1 deletion in differentiating T_{FR} revealed increased phosphorylation of STAT3 (pSTAT3) and decreased phosphorylation of STAT5 (pSTAT5) in all CD25-expressing T_{FR} subsets without further

cytokine-mediated activation (Figure 5G), suggesting that Blimp1 may repress IL-23R-STAT3 signaling while retaining the CD25-STAT5 pathway in T_{FR} cells.

Silencing IL-23R-STAT3 Signaling Rescues the Blimp1-Deficient T_{FR} Phenotype

We then asked whether forced reduction of IL-23R-STAT3 activation in Blimp1-deficient T_{FR} cells could remedy T_{FR} instability. We used lentiviral vectors that expressed the Thy1.1 reporter and small hairpin RNA (shRNA) targeting the *Il23r* gene to knock down IL-23R expression in Blimp1-deficient Treg before transfer of sorted Thy1.1$^+$ Treg and naive CD4+ T cells *(CD45.1$^+$)* into *Tcra*$^{-/-}$ hosts and immunization with NP-OVA (Figure 6A). Ten days later, we noted that transferred IL-23R-shRNA *(Thy1.1$^+$)* FoxP3$^+$ Treg expressed diminished levels of IL-23R and Bcl6 (Figure S5A), while the frequency of T_{FH} and GC B cells and anti-NP Ab titers were reduced (Figures 6B, 6C, and S5B). The expression of CD25, Helios, and granzyme B (i.e., genes associated with suppressive activity) was markedly increased (Figures S5A and S5C), while the expression of RORγt, IL-17A, and IFNγ was substantially reduced in Blimp1-deficient T_{FR} cells following IL-23R knockdown (Figures 6B, 6C, S5B, and S5C). These findings indicated that silencing IL-23R could rescue suppressive activity and restore the phenotype of Blimp1-deficient T_{FR} cells.

We also analyzed *Stat3*$^{fl/fl}$*Prdm1*$^{fl/fl}$*FoxP3*^{Cre} mice, which deleted both Blimp1 and STAT3 in FoxP3$^+$ T cells (Figure S5D), to determine whether impaired STAT3 activity in Blimp1-deficient T_{FR} cells could also remedy T_{FR} instability. These mice had decreased T_{FR}, T_{FH}, and GC B cell frequencies, reduced anti-NP Ab titers, minimal ectopic IL-17A, and increased FoxP3 expression by T_{FR} cells compared to *Prdm1*$^{fl/fl}$*FoxP3*^{Cre} mice after immunization (Figures 6D–6F, S5E, and S5F). Although the ratios of T_{FH}:T_{FR} or GC B:T_{FR} have been positively correlated with the strength of immune responses (Sage et al., 2013; Sage and Sharpe, 2015), our results did not reveal significant differences in the T_{FH}:T_{FR} ratios for each group (Figure S5G). The ratios of GC B:T_{FR} cells were negatively correlated with the Ab response, most likely reflecting the robust expansion of dysfunctional T_{FR}. These data suggested that the genetic status of T_{FR} cells should be considered when evaluating the relation between T_{FH}:T_{FR} ratios and immune response outcomes. These results indicated that reduction of the IL-23R-STAT3 axis could rescue the Blimp1-deficient T_{FR} phenotype and restore suppressive activity.

Increased STAT5 Activation in Differentiating Blimp1-Deficient T_{FR} Cells Restores Lineage Stability

Finally, we asked whether increased STAT5 activation in differentiating Blimp1-deficient T_{FR} cells could also mitigate T_{FR} instability. We transduced Blimp1-deficient Treg with a retroviral vector expressing GFP alone (control) or GFP plus constitutively active STAT5 (STAT5^{ca}) before the transfer of GFP$^+$ Treg with CD45.1$^+$ naive CD4$^+$T cells into *Tcra*$^{-/-}$ hosts, followed by immunization with NP-OVA (Figure S6A). Before transfer or 10 days post-immunization, we observed higher pSTAT5 levels in Treg expressing STAT5^{CA} compared with cells transduced with a control vector (Figures S6D). Expression of STAT5^{ca} in Blimp1-deficient Treg was associated with increased FoxP3 and CD25 expression, reduced T_{FH} and GC B cells (albeit no significance was detected), and diminished production of IL-17A and IFNγ by CD45.2$^+$ (STAT5^{CA}-transduced) T_{FR} compared with

T_{FR} cells transduced with control vector (Figures S6B–S6D), suggesting that the forced activation of STAT5 during T_{FR} differentiation can at least partially rescue Blimp1-deficient T_{FR} instability.

These results suggest that the essential contribution of Blimp1 to T_{FR} lineage stability and suppressive activity may reflect repression of the IL-23R-STAT3 axis and maintenance of the CD25-STAT5 pathway.

DISCUSSION

By virtue of their GC-specific localization, T_{FR} cells represent a phenotypically and functionally specialized Treg population that controls the GC and Ab response. Although T_{FR} cells share several features with T_{FH} and Treg, our understanding of the molecular and genetic elements that direct the differentiation of this specialized subset has been incomplete. Here, we have uncovered an essential contribution of the Blimp1 TF to T_{FR} cell differentiation, lineage stability, proper GC localization, and suppressive activity.

The Blimp1 gene is strongly expressed by almost all eTreg (Cretney et al., 2013), including FoxP3+ T_{FR} cells in B cell follicles (Linterman et al., 2011). Early studies of the contribution of Blimp1 to $CD4^+$ T cells that analyzed mice containing a systemic or T cell-specific deletion of Blimp1 have identified the contribution of Blimp1 to T cell expression of IL-10 (Cretney et al., 2011; Kallies et al., 2006; Martins et al., 2006). Histological analysis of non-lymphoid tissues, including lung, skin, and adipose tissues, in mice that carry a FoxP3-specific deletion of Blimp1 failed to reveal obvious abnormalities, with the exception of a mild hyperproliferative colitis apparent at 5 months of age. In contrast, the major phenotype of $Prdm1^{fl/fl}FoxP3^{Cre}$ mice was a markedly dysregulated Ab response, which included elevated IgE and autoantibody levels and the expansion of T_{FH} and GC B cells. We used multiple experimental settings for this analysis, including direct examination of $Prdm1^{fl/fl}FoxP3^{Cre}$ and heterozygous female $Prdm1^{fl/fl}FoxP3^{YFP\text{-}Cre+/-}$ mice, adoptive transfer of T_{FR}, inducible deletion of Blimp1 in T_{FR}, and a comparison of the T_{FH}-GC response of $Bcl6^{fl/fl}Prdm1^{fl/fl}FoxP3^{Cre}$ mice with $Prdm1^{fl/fl}FoxP3^{Cre}$, $Bcl6^{fl/fl}FoxP3^{Cre}$, and $FoxP3^{Cre}$ (WT) mice. We found that Blimp1 was essential for the maintenance of a stable T_{FR} phenotype, suppressive control of Ab responses, and avoidance of atopic IgE and autoantibody responses. Reduced expression of FoxP3 and diminished levels of receptors that normally contribute to T_{FR} inhibitory activity, including CTLA-4, were associated with increased numbers of T_{FH} and GC B cells in the steady state and after immunization. Our results also suggest that Blimp1-deficient T_{FR} rather than Blimp1-deficient non-T_{FR} Treg account for the abnormal immune phenotype of $Prdm1^{fl/fl}FoxP3^{Cre}$ mice.

Mutations resulting in diminished *FOXP3* expression that result in immune dysregulation (an X-linked [IPEX] syndrome) and genetic deletion of CTLA-4 in Treg are also marked by the loss of humoral tolerance and high serum IgE levels (Bennett et al., 2001; Wildin et al., 2001; Wing et al., 2014). We suggest that reduced FoxP3 expression by Blimp1-deficient T_{FR} secondary to an imbalance in STAT5/STAT3-based signaling may account in part for this abnormal phenotype. The expansion of Blimp1-deficient T_{FR} cells was marked by increased T_{FR} proliferation and reduced apoptosis. Depletion of STAT3 in Blimp1-deficient

T_{FR} decreased T_{FR} numbers to levels similar to those of WT T_{FR}, which is consistent with the ability of activated STAT3 to promote T cell proliferation and impede apoptosis (Akira, 2000). The expanded Blimp1-deficient T_{FR} population did not mediate significant suppressive activity and displayed a distorted cellular phenotype.

Diminished FoxP3 expression was accompanied by reduced levels of critical Treg gene products, including CTLA-4, CD25, and GITR, and increased production of the pro-inflammatory cytokines IFNγ and IL-17A. Previous studies have noted that even slight reductions in FoxP3 expression can profoundly affect Treg lineage stability and immunologic function (Di Pilato et al., 2019; Wan and Flavell, 2007). We and others have previously noted that the IL-2-STAT5 axis is essential to this process, reflecting in part an interaction between STAT5 and the *FoxP3 CNS2* region (Feng et al., 2014; Kim et al., 2015). However, the contribution of the IL-2-STAT5 axis to T_{FR} differentiation is more complex, reflecting its role in the early (*CD25*$^{+}$) and later GC-localized CD25$^{lo/-}$ T_{FR} cells. The latter T_{FR} effector subpopulation expresses low but significant levels of Blimp1 compared to their naive Treg precursors (Wing et al., 2017). We suggest that dynamic changes in Blimp1 expression, partly in response to environmental IL-2, accompany functional T_{FR} differentiation and appropriate navigation from the IL-2-rich T cell zone into IL-2-poor B cell follicles and final localization into the GC (Smigiel et al., 2014). In contrast, upregulation of CXCR5 and strong downregulation of CCR7 may increase the lineage instability of T_{FR} cells devoid of Blimp1 after genetic deletion. Production of pro-inflammatory cytokines by unstable Blimp1-deficient T_{FR} cells may reflect the upregulation of the IL-23R-STAT3 axis, expression of RORγt and IL-17A, and conversion into T_H17-like cells. Unstable Blimp1-deficient T_{FR} may also acquire the characteristics of T_{FH} cells, including the expression of IL-4, Bcl6, CXCR5, and IL-21.

In summary, we find that coordinate regulation of the IL-23R-STAT3 and CD-25-STAT5 axes by Blimp1 is essential for the maintenance of T_{FR} stability and suppressive activity. Identification of the molecular factors and signaling pathways that modulate Blimp1 expression in T_{FR} may allow the development of agents that modulate Ab responses in the context of vaccines and autoimmune disease.

STAR★METHODS

LEAD CONTACT AND MATERIALS AVAILABILITY

Further information and requests for resources and reagents should be directed to and will be fulfilled by the Lead Contact, Harvey Cantor (Harvey_Cantor@dfci.harvard.edu). Unique/stable reagents generated in this study are available from the Lead Contact with a completed Materials Transfer Agreement. Microarray data (GEO: GSE101611) have been deposited in the NCBI GEO.

EXPERIMENTAL MODEL AND SUBJECT DETAILS

Mice—C57BL/6J (B6), *Prdm1*$^{fl/fl}$ *FoxP3*$^{YFP\text{-}Cre}$ (*FoxP3*^{Cre}), *Rosa26*$^{Cre\text{-}ERT2}$ (iCre^{+}), *Bcl6*$^{fl/fl}$, *Stat3*$^{fl/fl}$, *Tcra*$^{-/-}$(Jackson Labs), *Rag2*$^{-/-}$, B6SJL (CD45.1) (Taconic Farms), and B6.FoxP3-GFP reporter mice were housed in pathogen-free conditions. *Prdm1*$^{fl/fl}$ mice were

bred onto *FoxP3*^{Cre} or *Rosa26*$^{Cre\text{-}ERT2}$ (iCre^{+}) mice to generate *Prdm1*$^{fl/fl}$*FoxP3*^{Cre}, *Prdm1*$^{fl/+}$*FoxP3*^{Cre}, or *Prdm1*$^{fl/fl}$*Rosa26*$^{Cre\text{-}ERT2}$ (*Prdm1*$^{fl/fl}$*iCre*$^{+}$) mice, respectively. *Bol6*$^{fl/fl}$ mice were bred onto *FoxP3*^{Cre} to generate *Bol6*$^{fl/fl}$*FoxP3*^{Cre} mice that were further crossed onto *Prdm1*$^{fl/fl}$*FoxP3*^{Cre} to yield *Bol6*$^{fl/fl}$*Prdm1*$^{fl/fl}$*FoxP3*^{Cre} mice. *Sfaf3*$^{fl/fl}$ mice were crossed onto *Prdm1*$^{fl/fl}$*FoxP3*^{Cre} to yield *Stat3*$^{fl/+}$*Prdm1*$^{fl/fl}$*FoxP3*^{Cre} or *Stat3*$^{fl/fl}$*Prdm1*$^{fl/fl}$*FoxP3*^{Cre} mice. All mice were used at the age of 6 to 9 weeks unless otherwise specified. Both sexes (males or females) were randomly included for all experiments in an unblinded fashion. Generally between 3 to 7 mice were used per group, as indicated in each experiment. All experiments were performed in compliance with federal laws and institutional guidelines as approved by DFCI's and UAB's Animal Care and Use Committee.

Cell Lines—293 T cells (CRL-3216, ATCC) were grown in DMEM supplemented with 10% FBS at 5% CO_2 at 37°C.

METHOD DETAILS

Flow Cytometry and Sorting—Fluorescence dye labeled Abs specific for mouse CD4 (GK1.5, RM4–5), TCRβ (H57–597), CD3 (145–2C11), CD25 (PC61), CD69 (H1.2F3), GITR (DTA-1), CTLA4 (UC10–4B9), KLRG1 (2F1/KLRG1), Blimp1 (5E7), TIGIT (1G9), RORγt (B2D), CCR6 (29–2L17), ST2 (RMST2–2, DIH9), Granzyme B (NGZB, GB11), IL-23R (12B2B64), Bcl2 (3F11), Helios (22F6), Ki-67 (SolA15), CD138 (281–2), CD45.1 (A20), CD45.2 (104), CD19 (1D3), B220 (RA3–6B2), CD44 (IM7), CD62L (MEL-14), Fas (15A7), IgM (II/41), T- and B cell activation antigen (GL7), ICOS (C398.4A), PD-1 (J43, 29F.1A12), CD90.1 (OX-7), IFN-γ (XMG1.2), IL-10 (JES5–16E3), IL-4 (11B11), IL-17A (eBio17B7), Bcl6 (K112–91), FoxP3 (FJK-16 s) and Bim (C34C5) were purchased from BD Biosciences, eBioscience, Biolegend and Cell Signaling Technology. Analysis of CXCR5 expression was performed using a biotinylated anti-CXCR5 (2G8, BD) Ab followed by incubation with APC or APC.Cy7 labeled streptavidin (Biolegend) as previously described (Leavenworth et al., 2015). A short incubation of cells with anti-mouse CD16/CD32 Fc block (BD) was performed prior to surface staining. Intracellular staining for Bcl6, FoxP3 and cytokines was performed using the FoxP3 staining buffer set (eBioscience). To assess pSTAT5 and pSTAT3 levels directly *ex vivo,* spleens and mLNs were immediately disrupted using glass slides into Cytofix/Cytoperm buffer (BD) for incubation of 30min at room temperature. The cells were washed and resuspended in 90% methanol and incubated on ice for 30min. After additional wash, the cells were stained for surface and intracellular antigens, including pSTAT5 (47/Stat5, pY694) and pSTAT3 (4/P-STAT3, pY705) for 45 min at room temperature (Smigiel et al., 2014). To assess apoptosis, cells were surface stained as described above, washed, and stained with Annexin-V (BD Biosciences) in 1 × Annexin Binding Buffer (BD Biosciences) for 15 min at room temperature, and immediately analyzed by FACS. For IL-21, intracellular staining was performed as previously described (Kashiwakuma et al., 2010). Cells were acquired on a Fortessa X20 using FACSDiva software (BD Biosciences) and analyzed with FlowJo software (Treestar). For cell sorting, single-cell suspension underwent positive enrichment for CD4^{+}T cells or B cells through the use of CD4or CD19 microbeads (Miltenyi Biotec). Enriched cells were labeled with various

fluorescent antibodies, as indicated in Figure S2, followed by sorting on a FACSAria II using FACSDiva software (BD Biosciences).

Adoptive Transfer and Immunization—As detailed in individual figure legends, FACS-sorted $CD4^+$ T cell subsets and/ or $GL7^-$ B cells were transferred into the indicated hosts before immunization with protein antigens (NP-OVA) emulsified in CFA or alum for an additional 7 days before euthanisia and ex vivo analysis. In some experiments, the hosts were further challenged with protein antigens in IFA at the indicated times. All immunizations were conducted by intraperitoneal injection. Serum was prepared at the indicated time for measurement of primary and secondary antibody titers.

Tamoxifen Treatment—For *in vivo* experiments involving Cre strains, mice were injected with 1 mg/25g body weight tamoxifen (Sigma) emulsified in sunflower oil (Sigma) intraperitoneally (vol: 100–150 ul) once every 24 hours for 3–4 consecutive days unless otherwise specified.

Enzyme-Linked Immunosorbent Assay (ELISA)—Detection of NP-specific antibodies was performed as described (Kim et al., 2010). Anti-nuclear Antibodies (ANA) in mouse sera were determined by ELISA (Alpha Diagnostic International). IgE was measured using the OptEIA ELISA kit (BD Biosciences).

Generation of Retrovirus and Lentivirus—The retroviral vector RV-pMIG expressing $STAT5^{ca}$ was a gift from Shane Crotty (Johnston et al., 2012). The production of retroviruses was performed as previously described (Leavenworth et al., 2015). The short hairpin RNA targeting the *Il23r* gene was cloned into the pLKO.3 Thy1.1 lentiviral vector (Addgene 14749). Lentiviral stocks were generated by transfection of 293T cells with this plasmid along with the lentiviral packaging vectors, PsPAX2 (Addgene 12260) and pCMV-VSV-G (Addgene 8454) (Stewart et al., 2003), through the use of TransIT-LT1 transfection reagent (Mirus). Viral supernatants were collected 72 h later before infection of Treg cells as described below.

Infection by Retrovirus and Lentivirus—Retroviral or lentiviral infection of Treg cells was adapted, as previously described (Leavenworth et al., 2015). Briefly, purified CD25+CD4+ T cells were stimulated with plate-bound anti-CD3 (5 μg ml^{-1}) and anti-CD28 (5 mg ml^{-1}) in the presence of 50 U ml^{-1} recombinant human IL-2 (rhIL-2, Peprotech). Three days post-stimulation, cells were infected with retrovirus expressing GFP alone or GFP plus $STAT5^{ca}$ or lentivirus expressing Thy1.1 or Thy1.1 plus IL-23R-shRNA, and sorted GFP^+ or $Thy1.1^+$ Treg along with $CD45.1^+$ naive $CD4^+$ T cells were transferred into $Tcra^{-/-}$ hosts followed by immunization.

ChIP-qPCR—B6.FoxP3-GFP mice were immunized with NP-OVA in CFA for 7 days. $GFP^+CD25^{hi}CD4^+$ Treg cells were sorted and fixed for 10 min at 37°C with 1% formaldehyde. Cells were washed twice in ice-cold PBS and cell pellets were stored at −80°C. Chromatin was isolated and immunoprecipitated with antibody to Blimp1 (Santa Cruz, sc-66015), acetylated H3 (AcH3) (Millipore, 06–599) or H3K27me3 (Abcam, ab-6002) and protein G Dynabeads (Thermo Fisher), followed by reverse crosslinking and

DNA purification. Quantitative real-time PCR assays were performed for Blimp1, AcH3 or H3K27me3 on Blimp1-binding sites at the indicated gene loci.

Generation of Bone Marrow Chimeras—*Rag2*$^{-/-}$ mice received a sublethal dose of radiation (600 rads) one day before BM cell transfer. BM cells from donor mice were harvested and depleted of NK1.1^{+}, CD4^{+}, CD8^{+} and B220^{+} cells using biotinylated antibodies targeting each subset and anti-biotin microbeads (Miltenyi Biotech). Enriched 5 × 10^{6}–10^{7} cells were intravenously injected into *Rag2*$^{-/-}$ mice. BM cells from *Prdm1*$^{fl/fl}$ and CD45.1 mice, or *Prdm1*$^{fl/fl}$*FoxP3*^{Cre} and CD45.1 mice (5 × 10^{6} cells per strain) were transferred, respectively.

Gene Expression Profiling—T_{FR} cells (PD-1^{+}CXCR5^{+}YFP^{+}CD4^{+}CD3^{+}) were sorted from *FoxP3*^{Cre} or *Prdm1*$^{fl/fl}$*FoxP3*^{Cre} mice 7 d post-immunization with NP-OVA in CFA. RNA was prepared with the RNeasy plus micro kit, according to the manufacturer's instructions (QIAGEN). RNA amplification, labeling, and hybridization to Mouse Gene 2.0 ST arrays (Affymetrix) were performed at a Core Facility (Dana Farber Cancer Institute).

***In Vitro* Suppression Assay of T_{FR} Cells—**The suppression assay of T_{FR} cells was performed as previously described (Sage et al., 2013). Briefly, sorted GL7^{-} B cells were cultured alone, or with T_{FH} cells in the presence or absence of T_{FR} cells from *FoxP3*^{Cre}or *Prdm1*$^{fl/fl}$*FoxP3*^{Cre} mice plus 2 μg/ml soluble anti-CD3 (2C11, BD) and 5 μg/ml anti-IgM (Jackson Immunoresearch). Five days later, IgG in the supernatants was determined by ELISA (Sage et al., 2013).

Immunoblot—The procedure was performed as described previously (Leavenworth et al., 2015). The following antibodies were used: Blimp1 (Santa Cruz, sc-66015) and Actin (Sigma, A-3584).

Quantitative RT-PCR—RNA was extracted using an RNeasy plus micro kit (QIAGEN). Relative quantification real-time PCR was performed with TaqMan gene expression assays, *Bcl6* (Mm00477633_m1), *Prdm1* (Mm00476128_m1), *Rps18* (Mm02601777_g1) and RNA-to-CT™ 1-Step Kit (Life Technologies). All results were first normalized to those of the *Rps18* control and are presented as normalized expression for the sample relative to the appropriate comparison conditions, as indicated in the legends.

Immunohistochemistry—To assess immunopathology in multiple organs, mice were fixed with Bouin's solution (Sigma), and tissue sections were generated from paraffin-embedded tissues and stained with hematoxylin and eosin. For the identification of germinal centers, 7 μm acetone- fixed frozen sections from spleen were air-dried and labeled with phycoerythrin (PE)-conjugated anti-B220 antibody (BD, RA3–6B2) and FITC-conjugated anti-GL-7 antibody (BD, clone GL7). Quantification of GL7-FITC positively-stained areas using ImageJ software (NIH) was depicted as pixel^{2}/area: two diameters of each germinal center (GL7^{+}) were measured, and were divided into 2 to get R1 and R2. Each GC area was estimated according to the formula S = R1 × R2 × 3.14. All the GC areas calculated in one slide equal the total GC area. The mean GC area was calculated by dividing the total GC area by the GC numbers. For confocal analysis of T_{FR} and T_{FH} distribution in the GC, 7

weeks old mice were immunized with NP-OVA in CFA and spleens were collected 14 days post immunization. The spleens were handled and stained as previously described (Vanderleyden and Linterman, 2017). Briefly, spleens were treated with periodate (0.01 M $NaIO_4$)-lysine (0.075 M L-lysine)-paraformaldehyde (1%) for 3 hours at 4C, before incubating overnight with sucrose 30% at 4C. On the following day, spleens were washed with new sucrose 30% and remaining sucrose was removed by dab-drying with a tissue. The spleens were put into cryomold containing OCT® Cryoprotective embedding medium (Sakura Finetek Usa Inc) and placed on a 2-propanol-dry ice cooling bath. The frozen blocks were stored in −80C until sectioning (10μm), blocking (2% BSAand 10% goat serum in PBS), permeabilization (2% Triton-Xin PBS) and staining with hamster anti-mouse CD3ε (clone eBio500A2, eBioscience), Alexa Fluor 568-conjugated goat anti-hamster IgG (ThermoFisher Scientific); eFluor450-con- jugated rat anti-mouse/rat FoxP3 (clone FJK16S, eBioscience); Alexa Fluor 647 conjugated rat anti-mouse IgD (clone 11–26c.2a, BioLegend); rabbit anti-mouse Ki67 (ThermoFisher Scientific), and Alexa Fluor 488 conjugated goat anti-rabbit (ThermoFisher Scientific). Images were captured with a Leica SP5 confocal microscope.

QUANTIFICATION AND STATISTICAL ANALYSES

Statistical analyses were performed using two-tailed, unpaired Student's t test with GraphPad Prism V6 software. Error bars indicate mean ± SEM. A p value of < 0.05 was considered to be statistically significant (* $p < 0.05$, ** $p < 0.01$, *** $p < 0.001$, ****$p < 0.0001$). No exclusion of data points was used. Sample size was not specifically predetermined, but the number of mice used was consistent with previous experience with similar experiments.

DATA AND CODE AVAILABILITY

The microarray data have been deposited in the NCBI GEO under accession number GEO: GSE101611.

Supplementary Material

Refer to Web version on PubMed Central for supplementary material.

ACKNOWLEDGMENTS

We acknowledge C. Benoist and D. Mathis (pLKO.3 Thy1.1 plasmid), D. Trono (psPAX2 plasmid), B. Weinberg (pCMV-VSV-G plasmid), S. Crotty (STAT5^{ca} plasmid), D. Campbell (phospho-STAT staining protocol), H. Nakajima (IL-21 staining protocol), Y. Li and D. Pan (microarray analysis), and A. Angel (manuscript/figure preparation). This study was supported in part by grants from the NIH (AI48125/AI37562, H.C.), the LeRoy Schecter Research Foundation (H.C.), and the National Natural Science Foundation of China (81971482, E.S.); fellowships from Sahlgrenska Academy, the University of Gothenburg, and The Foundation Blanceflor Boncompagni Ludovisi, nee Bildt (H.R.), and the Benacerraf Fellowship in Immunology (L.W.); and start-up funds from the University of Alabama at Birmingham (J.W.L.).

REFERENCES

Akira S (2000). Roles of STAT3 defined by tissue-specific gene targeting. Oncogene 19, 2607–2611. [PubMed: 10851059]

Bennett CL, Christie J, Ramsdell F, Brunkow ME, Ferguson PJ, White-sell L, Kelly TE, Saulsbury FT, Chance PF, and Ochs HD (2001). The immune dysregulation, polyendocrinopathy, enteropathy, X-linked syndrome (IPEX) is caused by mutations of FOXP3. Nat. Genet 27, 20–21. [PubMed: 11137993]

Botta D, Fuller MJ, Marquez-Lago TT, Bachus H, Bradley JE, Weinmann AS, Zajac AJ, Randall TD, Lund FE, Leon B, and Ballesteros-Tato A (2017). Dynamic regulation of T follicular regulatory cell responses by interleukin 2 during influenza infection. Nat. Immunol 18, 1249–1260. [PubMed: 28892471]

Chung Y, Tanaka S, Chu F, Nurieva RI, Martinez GJ, Rawal S, Wang YH, Lim H, Reynolds JM, Zhou XH, et al. (2011). Follicular regulatory T cells expressing Foxp3 and Bcl-6 suppress germinal center reactions. Nat. Med 17, 983–988. [PubMed: 21785430]

Cretney E, Xin A, Shi W, Minnich M, Masson F, Miasari M, Belz GT, Smyth GK, Busslinger M, Nutt SL, and Kallies A (2011). The transcription factors Blimp-1 and IRF4 jointly control the differentiation and function of effector regulatory T cells. Nat. Immunol 12, 304–311. [PubMed: 21378976]

Cretney E, Kallies A, and Nutt SL (2013). Differentiation and function of Foxp3(+) effector regulatory T cells. Trends Immunol. 34, 74–80. [PubMed: 23219401]

Crotty S (2011). Follicular helper CD4 T cells (TFH). Annu. Rev. Immunol 29, 621–663. [PubMed: 21314428]

Crotty S (2014). T follicular helper cell differentiation, function, and roles in disease. Immunity 41, 529–542. [PubMed: 25367570]

Di Pilato M, Kim EY, Cadilha BL, Prüßmann JN, Nasrallah MN, Seruggia D, Usmani SM, Misale S, Zappulli V, Carrizosa E, et al. (2019). Targeting the CBM complex causes T_{reg} cells to prime tumours for immune checkpoint therapy. Nature 570, 112–116. [PubMed: 31092922]

Feng Y, Arvey A, Chinen T, van der Veeken J, Gasteiger G, and Rudensky AY (2014). Control of the inheritance of regulatory T cell identity by a cis element in the Foxp3 locus. Cell 158, 749–763. [PubMed: 25126783]

Garg G, Muschaweckh A, Moreno H, Vasanthakumar A, Floess S, Lepennetier G, Oellinger R, Zhan Y, Regen T, Hiltensperger M, et al. (2019). Blimp1 Prevents Methylation of Foxp3 and Loss of Regulatory T Cell Identity at Sites of Inflammation. Cell Rep. 26, 1854–1868.e5. [PubMed: 30759395]

Harada Y, Tanaka S, Motomura Y, Harada Y, Ohno S, Ohno S, Yanagi Y, Inoue H, and Kubo M (2012). The 3' enhancer CNS2 is a critical regulator of interleukin-4-mediated humoral immunity in follicular helper T cells. Immunity 86, 188–200.

Johnston RJ, Choi YS, Diamond JA, Yang JA, and Crotty S (2012). STAT5 is a potent negative regulator of TFH cell differentiation. J. Exp. Med 209, 243–250. [PubMed: 22271576]

Kallies A, Hawkins ED, Belz GT, Metcalf D, Hommel M, Corcoran LM, Hodgkin PD, and Nutt SL (2006). Transcriptional repressor Blimp-1 is essential for T cell homeostasis and self-tolerance. Nat. Immunol 7, 466–474. [PubMed: 16565720]

Kashiwakuma D, Suto A, Hiramatsu Y, Ikeda K, Takatori H, Suzuki K, Kagami S, Hirose K, Watanabe N, Iwamoto I, and Nakajima H (2010). B and T lymphocyte attenuator suppresses IL-21 production from follicular Th cells and subsequent humoral immune responses. J. Immunol 185, 2730–2736. [PubMed: 20660710]

Kim HJ, Verbinnen B, Tang X, Lu L, and Cantor H (2010). Inhibition of follicular T-helper cells by CD8(+) regulatory T cells is essential for self tolerance. Nature 467, 328–332. [PubMed: 20844537]

Kim HJ, Barnitz RA, Kreslavsky T, Brown FD, Moffett H, Lemieux ME, Kaygusuz Y, Meissner T, Holderried TA, Chan S, et al. (2015). Stable inhibitory activity of regulatory T cells requires the transcription factor Helios. Science 350, 334–339. [PubMed: 26472910]

Laidlaw BJ, Lu Y, Amezquita RA, Weinstein JS, Vander Heiden JA, Gupta NT, Kleinstein SH, Kaech SM, and Craft J (2017). Interleukin-10 from CD4+ follicular regulatory T cells promotes the germinal center response. Sci. Immunol 2, eaan4767. [PubMed: 29054998]

Laurence A, Amarnath S, Mariotti J, Kim YC, Foley J, Eckhaus M, O'Shea JJ, and Fowler DH (2012). STAT3 transcription factor promotes instability of nTreg cells and limits generation of iTreg cells during acute murine graft-versus-host disease. Immunity 37, 209–222. [PubMed: 22921119]

Leavenworth JW, Tang X, Kim HJ, Wang X, and Cantor H (2013). Amelioration of arthritis through mobilization of peptide-specific $CD8^+$ regulatory T cells. J. Clin. Invest 123, 1382–1389. [PubMed: 23376792]

Leavenworth JW, Verbinnen B, Yin J, Huang H, and Cantor H (2015). A p85a-osteopontin axis couples the receptor ICOS to sustained Bcl-6 expression by follicular helper and regulatory T cells. Nat. Immunol 16, 96–106. [PubMed: 25436971]

Linterman MA, Pierson W, Lee SK, Kallies A, Kawamoto S, Rayner TF, Srivastava M, Divekar DP, Beaton L, Hogan JJ, et al. (2011). Foxp3+ follicular regulatory T cells control the germinal center response. Nat. Med 17, 975–982. [PubMed: 21785433]

Martins GA, Cimmino L, Shapiro-Shelef M, Szabolcs M, Herron A, Magnusdottir E, and Calame K (2006). Transcriptional repressor Blimp-1 regulates T cell homeostasis and function. Nat. Immunol 7, 457–465. [PubMed: 16565721]

Minnich M, Tagoh H, Bonelt P, Axelsson E, Fischer M, Cebolla B, Tarakhovsky A, Nutt SL, Jaritz M, and Busslinger M (2016). Multifunctional role of the transcription factor Blimp-1 in coordinating plasma cell differentiation. Nat. Immunol 17, 331–343. [PubMed: 26779602]

Sage PT, and Sharpe AH (2015). T follicular regulatory cells in the regulation of B cell responses. Trends Immunol. 36, 410–418. [PubMed: 26091728]

Sage PT, Francisco LM, Carman CV, and Sharpe AH (2013). The receptor PD-1 controls follicular regulatory T cells in the lymph nodes and blood. Nat. Immunol 14, 152–161. [PubMed: 23242415]

Smigiel KS, Richards E, Srivastava S, Thomas KR, Dudda JC, Klonowski KD, and Campbell DJ (2014). CCR7 provides localized access to IL-2 and defines homeostatically distinct regulatory T cell subsets. J. Exp. Med 211, 121–136. [PubMed: 24378538]

Stewart SA, Dykxhoorn DM, Palliser D, Mizuno H, Yu EY, An DS, Sabatini DM, Chen IS, Hahn WC, Sharp PA, et al. (2003). Lentivirus-delivered stable gene silencing by RNAi in primary cells. RNA 9, 493–501. [PubMed: 12649500]

Vanderleyden I, and Linterman MA (2017). Identifying Follicular Regulatory T Cells by Confocal Microscopy. Methods Mol. Biol 1623, 87–93. [PubMed: 28589349]

Vasanthakumar A, Moro K, Xin A, Liao Y, Gloury R, Kawamoto S, Fagarasan S, Mielke LA, Afshar-Sterle S, Masters SL, et al. (2015). The transcriptional regulators IRF4, BATF and IL-33 orchestrate development and maintenance of adipose tissue-resident regulatory T cells. Nat. Immunol 16 276–285 [PubMed: 25599561]

Wan YY, and Flavell RA (2007). Regulatory T-cell functions are subverted and converted owing to attenuated Foxp3 expression. Nature 445, 766–770. [PubMed: 17220876]

Weinstein JS, Herman EI, Lainez B, Licona-Limón P, Esplugues E, Flavell R, and Craft J (2016). TFH cells progressively differentiate to regulate the germinal center response. Nat. Immunol 17, 1197–1205. [PubMed: 27573866]

Wildin RS, Ramsdell F, Peake J, Faravelli F, Casanova JL, Buist N, Levy-Lahad E, Mazzella M, Goulet O, Perroni L, et al. (2001). X-linked neonatal diabetes mellitus, enteropathy and endocrinopathy syndrome is the human equivalent of mouse scurfy. Nat. Genet 27, 18–20. [PubMed: 11137992]

Wing JB, Ise W, Kurosaki T, and Sakaguchi S (2014). Regulatory T cells control antigen-specific expansion of Tfh cell number and humoral immune responses via the coreceptor CTLA-4. Immunity 41, 1013–1025. [PubMed: 25526312]

Wing JB, Kitagawa Y, Locci M, Hume H, Tay C, Morita T, Kidani Y, Matsuda K, Inoue T, Kurosaki T, et al. (2017). A distinct subpopulation of $CD25^-$ T-follicular regulatory cells localizes in the germinal centers. Proc. Natl. Acad. Sci. USA 114, E6400–E6409. [PubMed: 28698369]

Highlights

- FoxP3-specific ablation of Blimp1 results in expansion of dysfunctional T_{FR} cells
- Inducible deletion of Blimp1 in T_{FR} cells impairs T_{FR} stability and function
- Blimp1 controls CTLA4 expression, IL-23R-CD25 and CXCR5-CCR7 axes in T_{FR} cells
- Blimp1 controls appropriate homing and positioning of T_{FR} cells into the GC

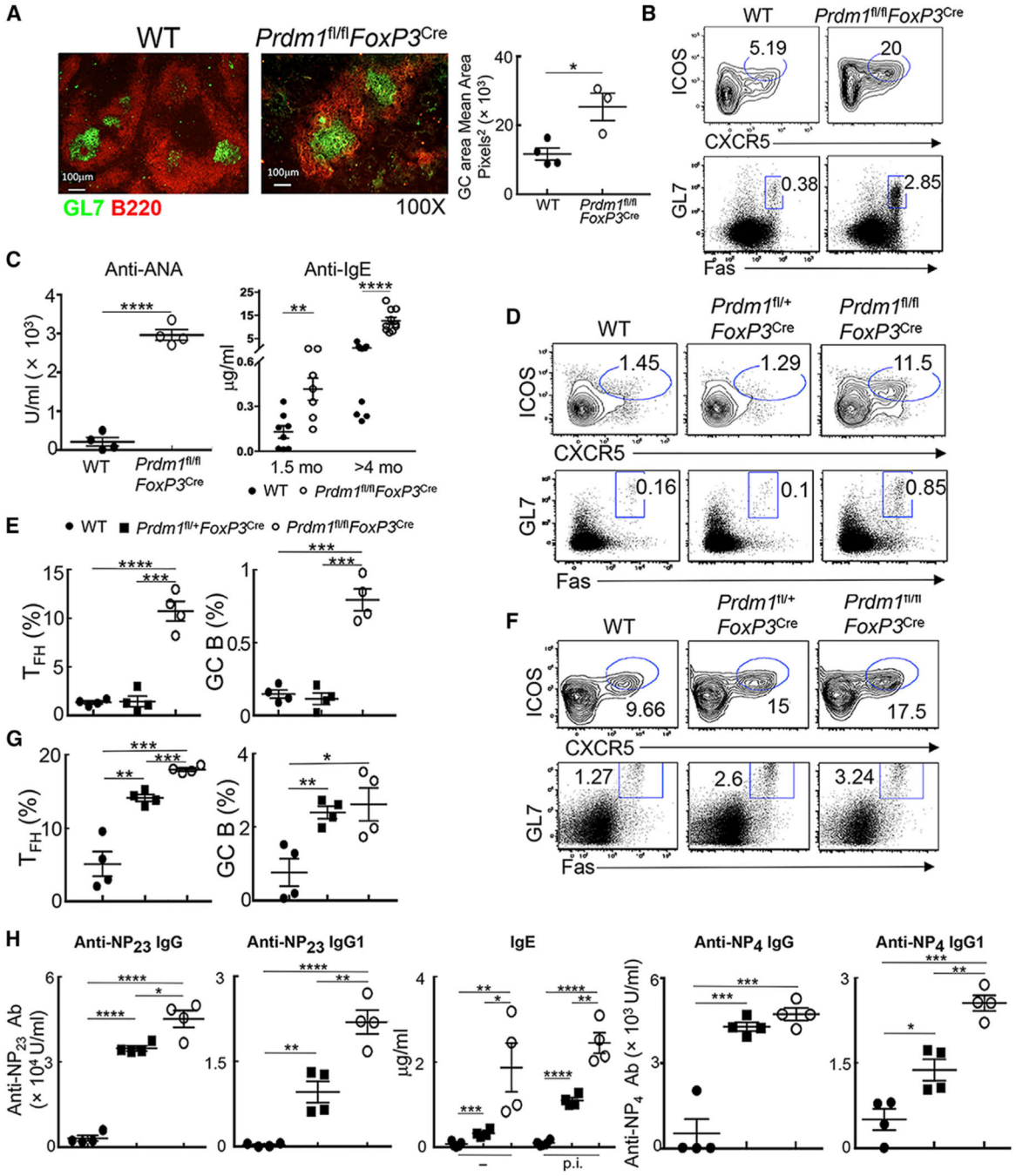

Figure 1. FoxP3-Specific Deletion of Blimp1 Leads to Dysregulated GC Responses

(A) Histology of splenic GCs, and quantification of $GL7^+$ GC areas from 4- to 5-month-old *FoxP3*^{Cre} (WT) and *Prdm1*$^{fl/fl}$*FoxP3*^{Cre} (KO) mice (n = 3–4/group).

(B) Flow cytometry of splenic T_{FH} ($CD4^+CD3^+ICOS^{hi}CXCR5^+FoxP3^-$) and GC B ($B220^+GL7^+Fas^+$) from 4- to 5-month-old mice.

(C) (Left) Serum ANA levels from 4- to 5-month-old mice (n = 4/group). (Right) Serum IgE levels from 1.5- and >4-month-old WT and KO mice (n = 7–11/group).

(D–G) Flow cytometry and frequency of splenic T_{FH} and GC B from 6-week-old mice before (D and E) or after (F and G) immunization with NP-KLH in complete Freund's adjuvant (CFA) (n = 4/group).

(H) Serum anti-NP23 Ig, anti-NP4 Ig, IgG1, and IgE levels from 6-week-old mice after immunization with NP-KLH in CFA (n = 4/group).

p.i., post immunization; −, before immunization. For (B)–(H), the data represent one of four independent experiments. *p < 0.05, **p < 0.01, ***p < 0.001, and ****p < 0.0001 (unpaired two-tailed Student's t test). Error bars indicate means ± SEMs.

See also Figure S1.

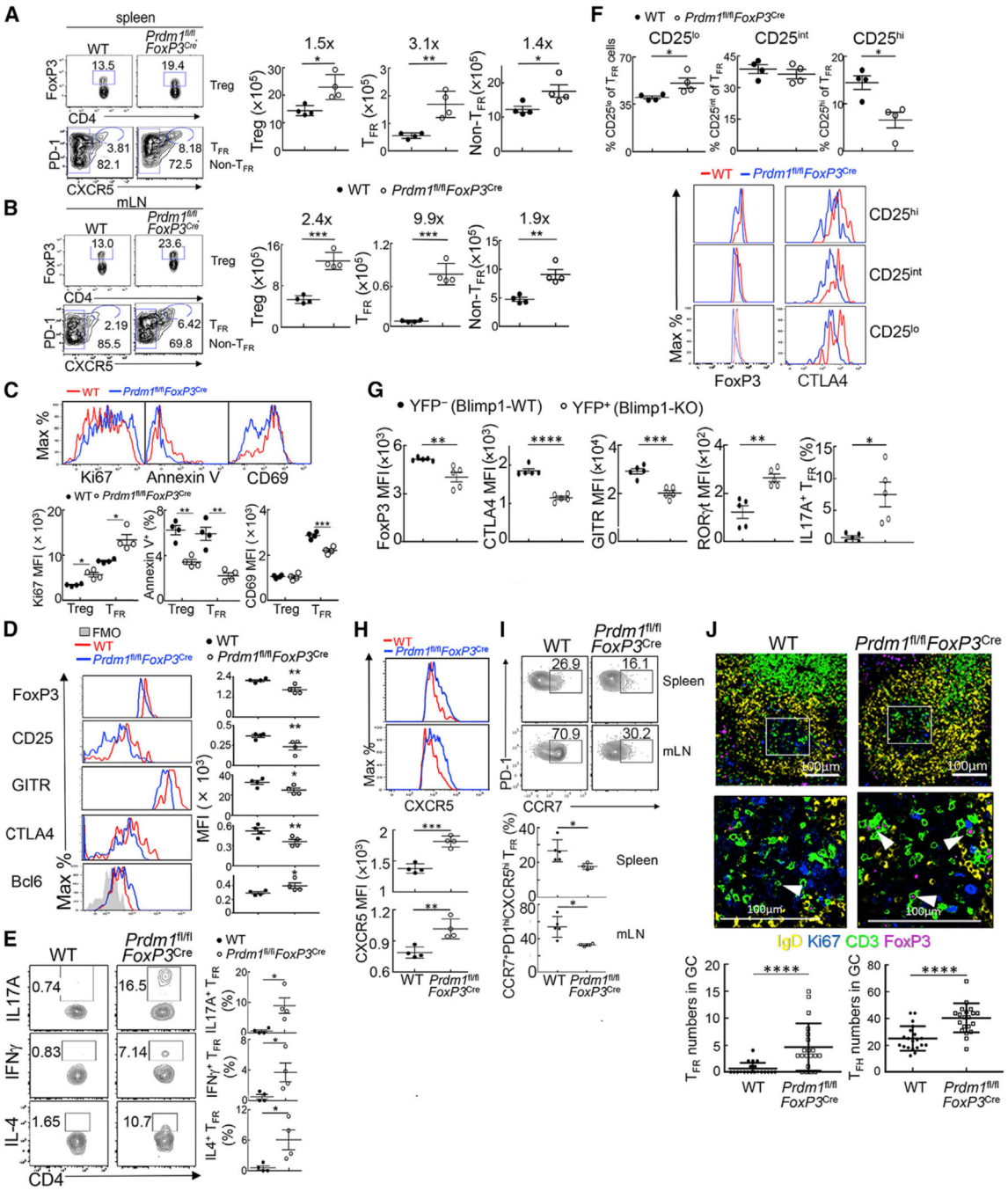

Figure 2. Expanded T_{FR} Cells Express an Abnormal Phenotype and Altered GC Distribution after Immunization of *Prdm1*$^{fl/fl}$*FoxP3*^{Cre} Mice

(A and B) Flow cytometry (left) and numbers (right) of splenic (A) or mLN (B) Treg ($FoxP3^+CD4^+$) (upper), T_{FR} ($CD4^+CD3^+PD\text{-}1^+CXCR5^+FoxP3^+$), and non-$T_{FR}$ ($CD4^+CD3^+CXCR5^-FoxP3^+$) (bottom) from WT and KO mice (7–9 weeks old) 10 days post-immunization with NP-KLH in CFA.

(C) Histogram of Ki67, annexin V, and CD69 expression in mLN T_{FR} cells in (B) (upper) and quantification of mean fluorescence intensity (MFI) in mLN T_{FR} and $CXCR5^-$ Treg cells (bottom).

(D) Expression of T_{FR}-associated gene products by splenic T_{FR} from (A) and quantification of MFI (right).

(E) IL-17A, IFNγ, and IL-4 expression (left) and frequency (right) by splenic T_{FR} ($CD4^+CD3^+PD\text{-}1^+BTLA^+FoxP3^+$) cells from WT or KO mice (6–8 weeks old) at day 7 post-immunization with NP-OVA in CFA.

(F) Frequency of $CD25^{lo}$ (left), $CD25^{int}$ (center), and $CD25^{hi}$ (right) splenic T_{FR} from WT and KO mice (6–8 weeks old) 10 days post-immunization with NP-OVA in CFA. (Bottom) FoxP3 and CTLA-4 expression in the CD25-expressing T_{FR} subsets.

(G) MFI of FoxP3, CTLA-4, GITR, and RORγt expression and frequencies of $IL\text{-}17A^+$ cells in YFP^+ Blimp1-deficient (KO) compared to YFP^- Blimp1-sufficient (WT) T_{FR} cells from the spleens of female $Prdm1^{fl/fl}FoxP3^{Cre/+}$ mice (6–8 weeks old) 10 days post-immunization with NP-OVA in CFA.

(H and I) CXCR5 (H) and CCR7 (I) expression in the splenic T_{FR} cells in (A) and mLN T_{FR} cells in (B).

(J) Histology of 7-week-old WT and KO mice 14 days post-immunization with NP-OVA in CFA. T_{FR} cells ($CD3^+FoxP3^+$, white arrows) and T_{FH} cells ($CD3^+FoxP3^-$) in the GC area ($Ki67^+$) within the B cell follicle (IgD^+). Insets indicate the B cell follicles. (Bottom) Numbers of T_{FR} and T_{FH} cells in the GC.

In (A)–(I), the data are representative of four independent experiments (A–F, n = 4/group; G, n = 5/group; H and I, n = 4–5/group). In (J), the data are representative of two independent experiments. *$p < 0.05$, **$p < 0.01$, ***$p < 0.001$, and ****$p < 0.0001$ (unpaired two-tailed Student's t test). Error bars indicate means ± SEMs.

See also Figure S2.

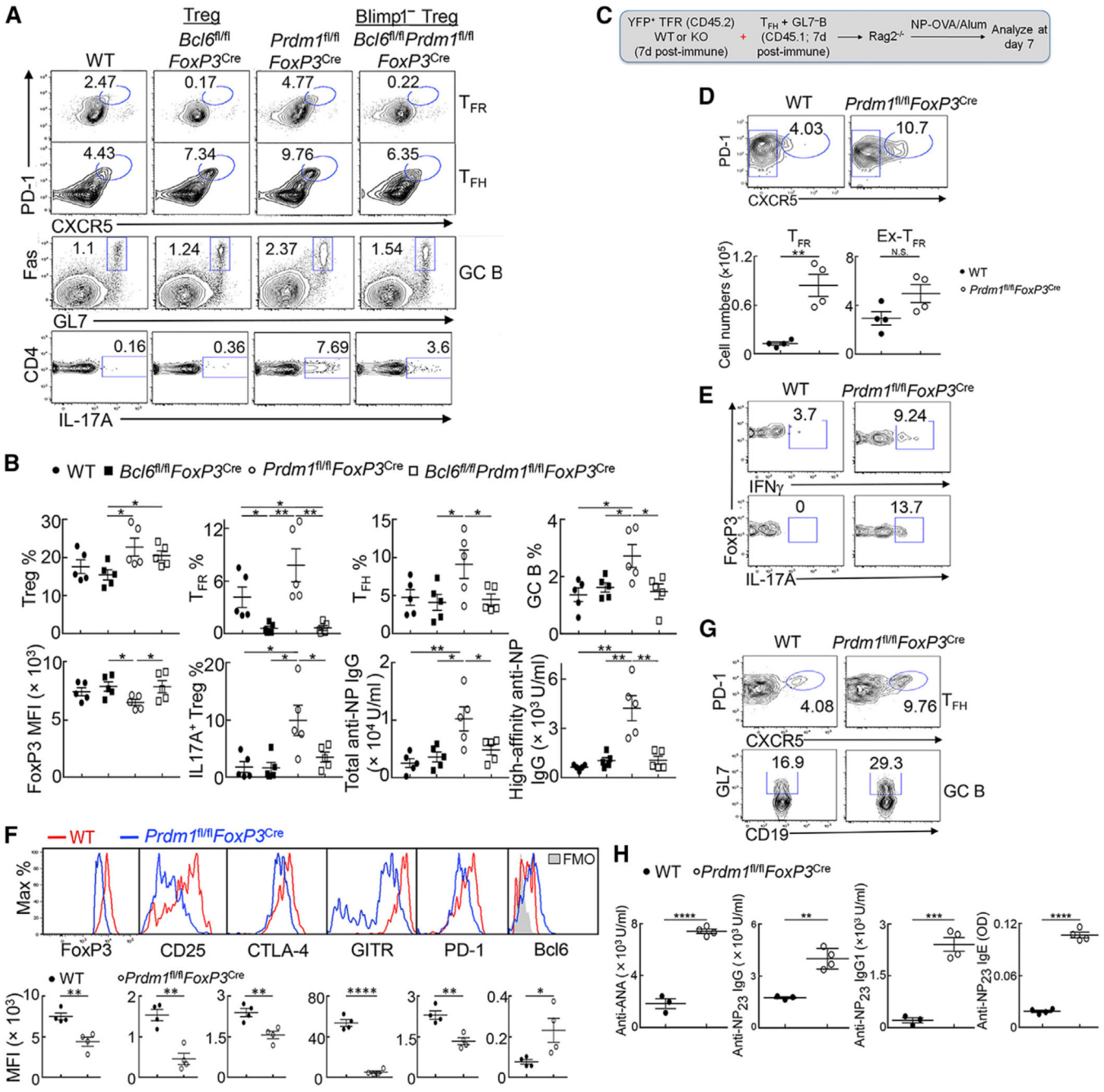

Figure 3. Blimp1 Deficiency Impairs T_{FR} Suppressive Activity and Alters Gene Expression by T_{FR} Cells

(A and B) Splenic T_{FR}, T_{FH}, GC B, and expression of IL-17A in Treg cells from the indicated mouse strains (6–8 weeks old) 10 days post-immunization with NP-OVA in CFA (A). Frequencies of Treg, T_{FR}, T_{FH}, GC B cells, and IL-17A$^+$ Treg cells, FoxP3 MFI, and total and high-affinity anti-NP IgG titers (B).

(C–G) (C) Schematic presentation of experimental protocol. CD45.2$^+$ WT, KO, and CD45.1$^+$ mice were immunized with NP-OVA in alum. Seven days later, sorted T_{FR} (CD4$^+$CD3$^+$PD-1$^+$CXCR5$^+$YFP$^+$) along with CD45.1$^+$ T_{FH}

($CD4^+CD3^+PD\text{-}1^+CXCR5^+GITR^-$) and $GL7^-$ B cells ($B220^+GL7^-$) were transferred into *Rag2*$^{-/-}$ hosts followed by immunization with NP-OVA in alum before analysis (day 7).

(D) Fluorescence-activated cell sorting (FACS) profile (upper) and numbers (bottom) of T_{FR} ($CD45.2^+CD4^+CD3^+PD\text{-}1^+CXCR5^+FoxP3^+$) and ex-$T_{FR}$ ($CD45.2^+CD4^+CD3^+CXCR5^-$) cells.

(E) Intracellular IL-17A and IFNγ expression by donor T_{FR} cells.

(F) Histogram (upper) and MFI (bottom) of the indicated markers by donor $CD45.2^+$ WT T_{FR} cells (red) and $CD45.2^+$ KO T_{FR} cells (blue).

(G) Flow cytometry of donor $CD45.1^+$ T_{FH} ($CD45.2^-CD4^+CD3^+PD\text{-}1^+CXCR5^+$) and GC B cells ($CD19^+GL7^+$) 7 days post-immunization.

(H) *Tcra*$^{-/-}$ mice were transferred with sorted T_{FR} (WT versus KO) along with $CD45.1^+$ T_{FH} cells, followed by immunization with NP-OVA in CFA. Serum ANA, anti-NP23 IgG, IgG1, and IgE levels were analyzed 10 days post-immunization.

In (A) and (B), the data are pooled from two independent experiments (n = 5/group). In (C)–(H), the data are representative of three independent experiments (D and F, n = 4/group; H, n = 3–4/group). N.S., no significance, *p < 0.05, **p < 0.01, ***p < 0.001, and ****p < 0.0001 (unpaired two-tailed Student's t test). Error bars indicate means ± SEMs.

See also Figure S2.

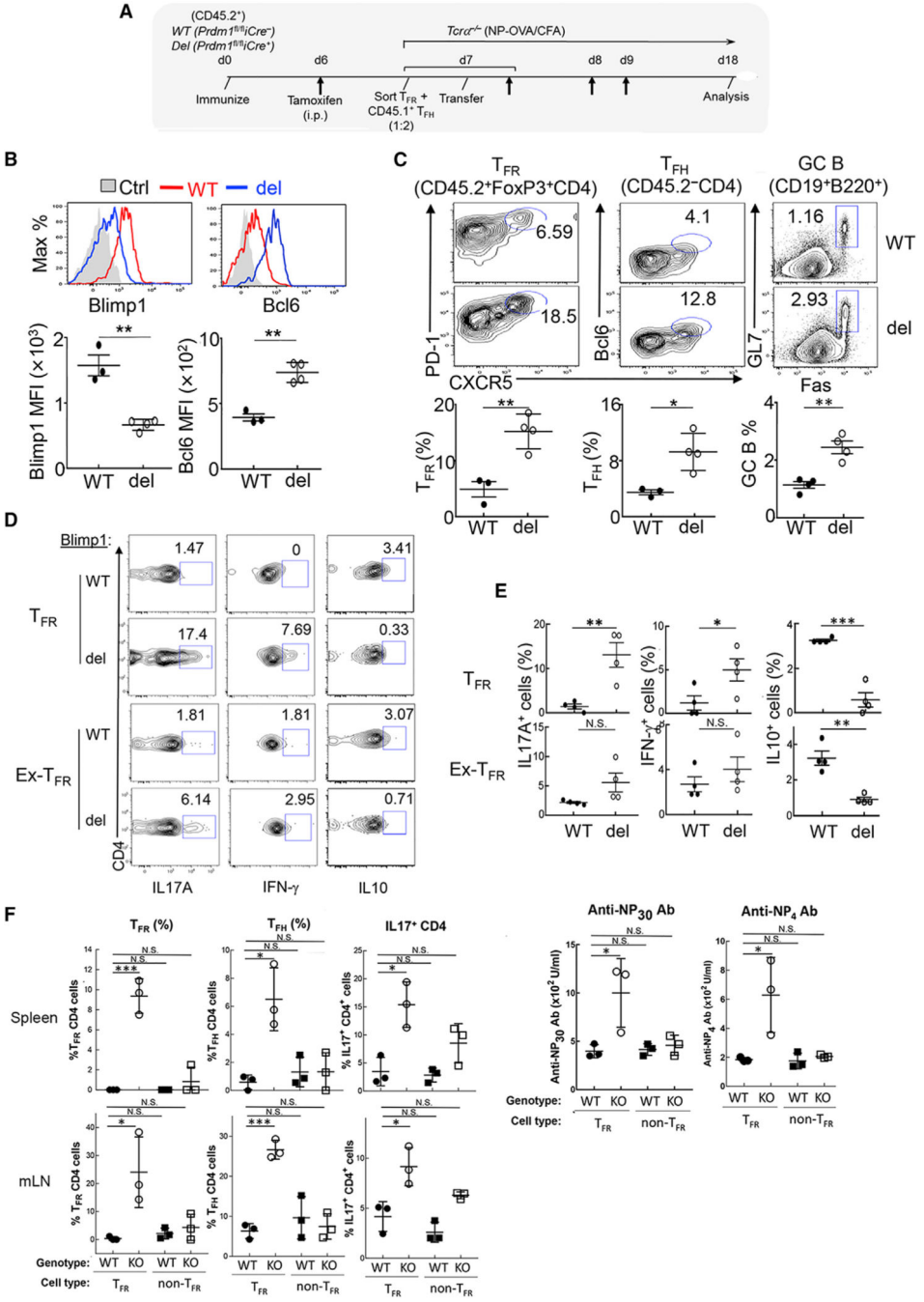

Figure 4. Blimp1 Deletion in T_{FR} Cells after Immunization Impairs T_{FR} Suppressive Activity

(A) Schematic diagram of experimental protocol. Donor CD45.2$^+$ *Prdm1*$^{fl/fl}$*iCre*$^-$ (WT), *Prdm1*$^{fl/fl}$*iCre*$^+$ (Blimp1-deleted; del), and CD45.1 $^+$ mice were immunized with NP-OVA in CFA for 7 days; tamoxifen was administered to WT and Del mice on day 6. On day 7, donors were euthanized and sorted *CD45.2*$^+$ T_{FR} (CD4$^+$CD3$^+$PD-1$^+$CXCR5$^+$GITR$^+$) along with CD45.1$^+$ T_{FH} cells (CD4$^+$CD3$^+$PD-1$^+$CXCR5$^+$GITR$^-$) were transferred into *Tcra*$^{-/-}$ hosts followed by immunization with NP-OVA in CFA and tamoxifen administration daily from days 7 to 9. Spleens from euthanized hosts were analyzed on day 18.

(B) Histogram (upper) and MFI (bottom) of Blimp1 and Bcl6 expression in donor CD45.2$^+$ T_{FR} cells after tamoxifen injection. Ctrl, T_{FR} cells from *Prdm1*$^{fl/fl}$*FoxP3*^{Cre} (left), or *Bcl6*$^{fl/fl}$*FoxP3*^{Cre} mice (right).

(C) Frequency of CD45.2$^+$ T_{FR} (CD45.2$^+$CD4$^+$PD-1$^+$CXCR5$^+$FoxP3$^+$), CD45.1$^+$ T_{FH} (CD45.2$^-$CD4$^+$Bcl6$^+$CXCR5$^+$), and GC B cells (B220$^+$CD19$^+$GL7$^+$Fas$^+$).

(D and E) Expression (D) and quantification (E) of IL-17A, IFNγ, and IL-10 by donor CD45.2$^+$ T_{FR} and ex-T_{FR} cells.

(F) WT and KO mice were immunized with NP-OVA in CFA. Seven days later, T_{FR} (WT versus KO: CD4$^+$CD3$^+$PD-1$^+$CXCR5$^+$YFP$^+$) and non-T_{FR} (WT versus KO: CD4$^+$CD3$^+$CXCR5$^+$YFP$^+$) were sorted and transferred (10^5/mouse) into *Tcra*$^{-/-}$ hosts followed by immunization with NP-OVA in CFA; hosts were further challenged with NP-OVA in IFA at day 13. Spleens or mLNs were analyzed on day 20 (n = 3/group). Splenic (upper) or mLN (center) T_{FR}, T_{FH}, intracellular expression of IL-17A by donor T_{FR} and non-T_{FR} cells. At right, serum anti-NP_{30} IgG, and anti-NP_4 IgG levels.

In (A)–(E), the data are representative of two independent experiments (B–E: n = 3–4/group). N.S., no significance, *p < 0.05, **p < 0.01, and ***p < 0.001 (unpaired two-tailed Student's t test). Error bars indicate means ± SEMs.

See also Figure S3.

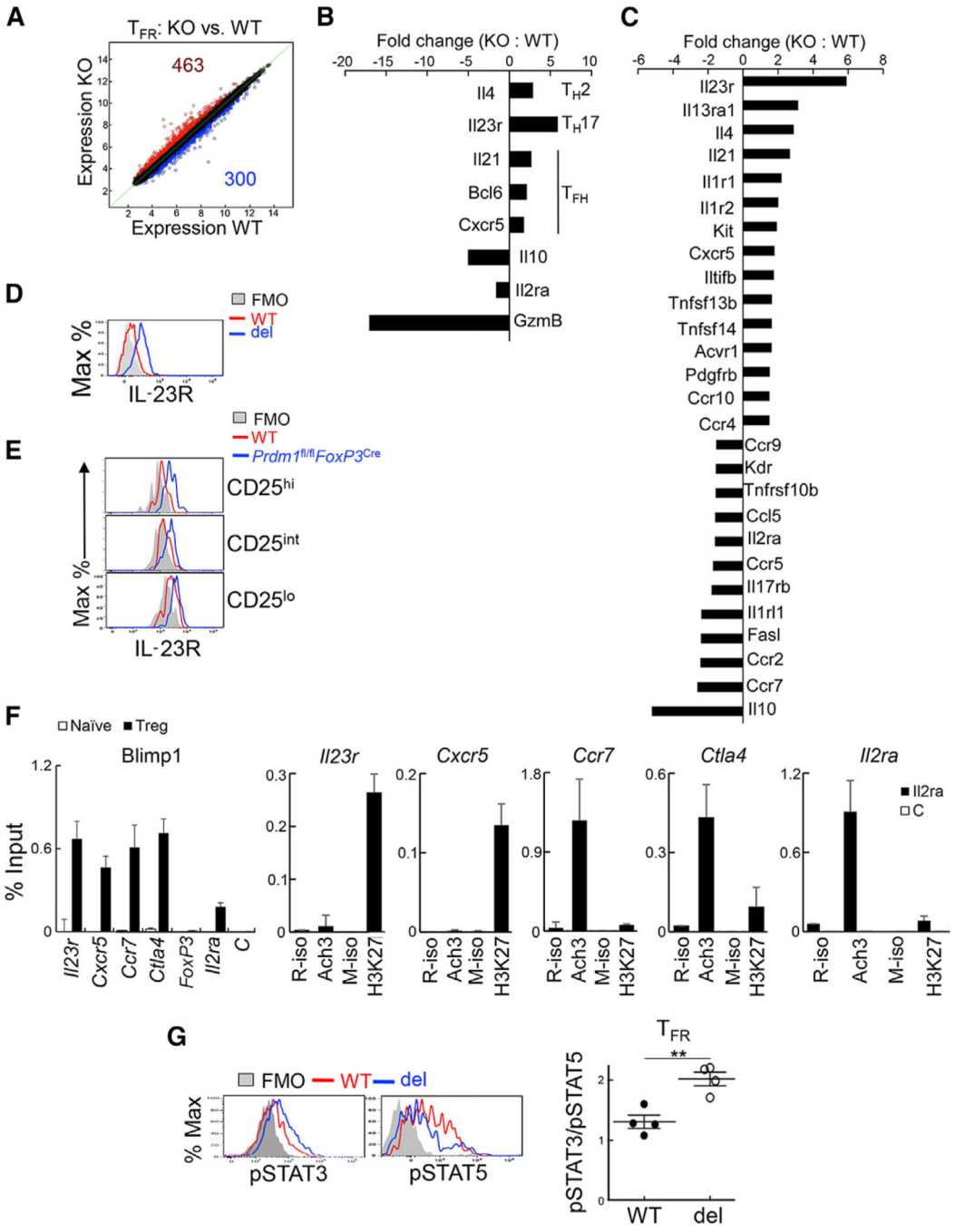

Figure 5. Mechanism of Blimp1-Dependent Control of T_{FR} Differentiation: Contribution of the IL-23R-STAT3 Axis and CXCR5-CCR7 Expression

(A) WT and KO mice (6 weeks old) were immunized with NP-OVA in CFA. Seven days later, T_{FR} cells ($CD4^+CD3^+PD\text{-}1^+CXCR5^+YFP^+$) were sorted for microarray analysis. Differential gene expression in T_{FR} from WT and KO mice (>1.5-fold) is shown.

(B) Pathway analysis revealed control of genes associated with T_H cell differentiation by Blimp1.

(C) Genes related to cytokine-cytokine receptor interaction by DAVID.

(D) IL-23R expression by donor T_{FR} cells in *Tcra*$^{-/-}$ hosts after tamoxifen-induced deletion of Blimp1, as in Figure 4.

(E) IL-23R expression in the CD25-expressing T_{FR} subsets from WT and KO mice (6–8 weeks old) 10 days post-immunization.

(F) FoxP3-GFP reporter mice were immunized with NP-OVA in CFA. Seven days later, Treg ($CD4^+CD3^+GFP^+CD25^+$) and $CD4^+$ naive T cells ($CD4^+CD3^+GFP^-CD44^-$) were sorted, chromatin prepared, and ChIP-PCR analyses performed for Blimp1, acetylated H3 (AcH3), and H3K27me3 at Blimp1-binding sites at the 3rd intron of *Il23r,* the 1st intron of *Cxcr5,* the 5′ distal element of *CTLA-4,* the 3rd intron of *Ccr7,* the *FoxP3 CNS2,* the 1st intron of *Il2ra,* and a non-specific region (C, control) of *Il2ra.* Data are shown as the percentage of input. Naive cells were used as controls for the anti-Blimp1 assay. Rabbit IgG isotype (R-iso) and mouse IgG isotype (M-iso) served as controls for the anti-AcH3 assay and anti-H3K27 assay, respectively.

(G) *Prdm1*$^{fl/fl}$*iCre*$^-$ (WT) and *Prdm1*$^{fl/fl}$*iCre*$^+$ (Del) mice (8 weeks old) were treated with tamoxifen at day 0, followed by immunization with NP-OVA in CFA at day 1 and injection of tamoxifen daily for 4 days. Expression of pSTAT3 and pSTAT5 in T_{FR} cells at day 7 post-immunization. At right, pSTAT3:pSTAT5 ratios in T_{FR} cells are shown (n = 4/group).

In (D), (E), and (G), the data represent one of two experiments. In (F), the data represent one of three independent experiments. **$p < 0.01$ (unpaired two-tailed Student's t test). Error bars indicate means ± SEMs.

See also Figure S4.

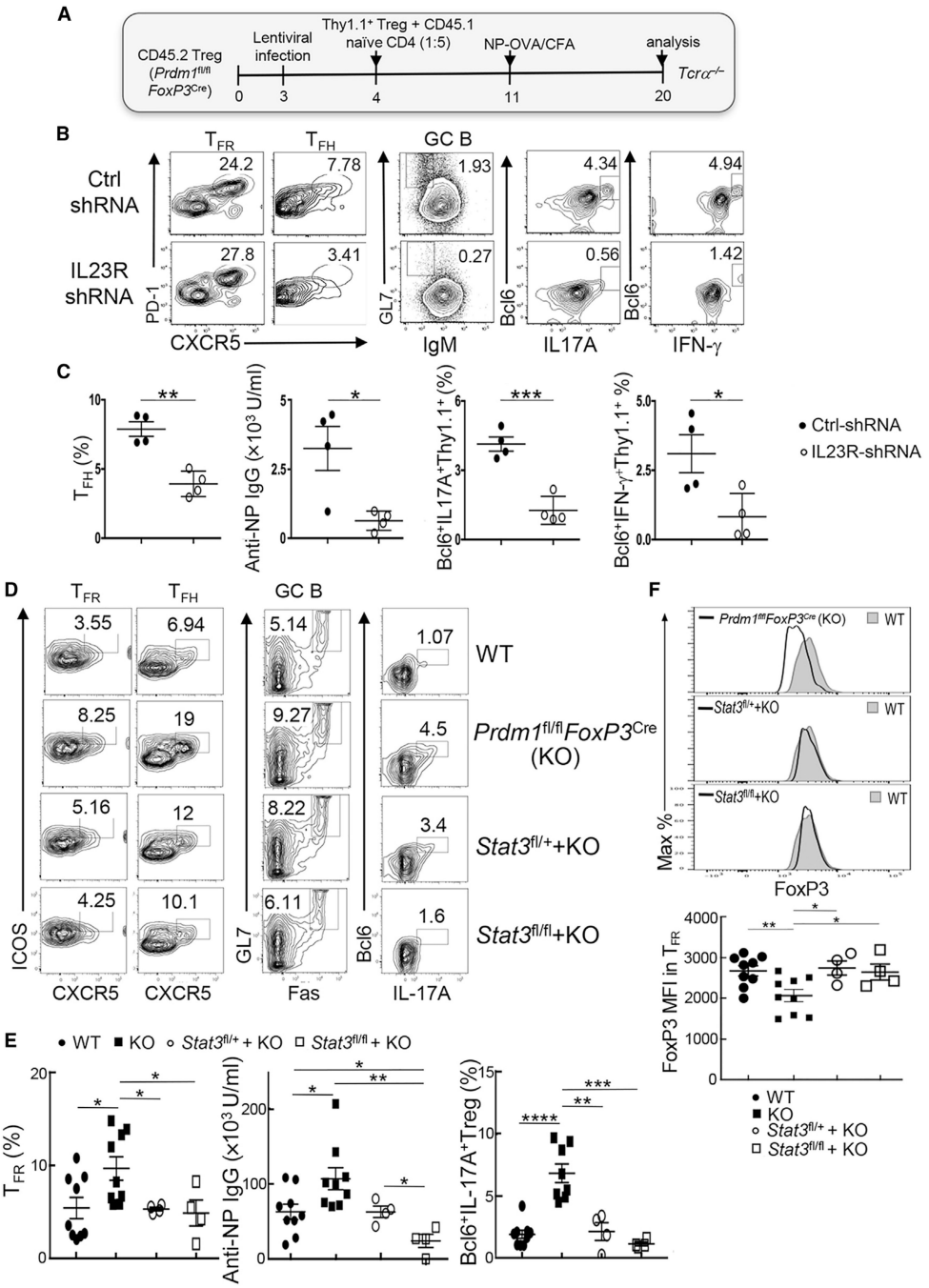

Figure 6. Silencing the IL-23R-STAT3 Axis Rescues the Blimp1-Deficient T_{Fr} Phenotype

(A) Schematic presentation of experimental protocol. KO Treg cells were sorted and cultured withanti-CD3andanti-CD28 plusIL-2for3days. Cells were infected with lentivirus expressing the Thy1.1 reporter plus IL-23R-shRNA or Ctrl-shRNA. On day 4, sorted Thy1.1$^+$ Treg along with CD45.1$^+$ naive CD4$^+$ T cells were transferred into *Tcra*$^{-/-}$ hosts followed by immunization with NP-OVA in CFA on day 11. Splenocytes were analyzed on day 20.

(B) Thy1.1^{+} T_{FR}, CD45.2^{-} Thy1.1^{-} T_{FH} and GL7^{+} B cells, IL-17A, and IFNγ production by Thy1.1^{+} T_{FR}.

(C) Frequency of CD45.2^{-} Thy1.1^{-} T_{FH}, Bcl6^{+} IL-17A^{+}, and Bcl6^{+} IFNγ^{+} in donor Thy1.1^{+} T_{FR} cells and in anti-NP IgG titers.

(D–F) WT, KO, *Stat3*$^{fl/+}$*Prdm1*$^{fl/fl}$*FoxP3*^{Cre} (*Stat3*$^{fl/+}$ + KO), and *Stat3*$^{fl/fl}$*Prdm1*$^{fl/fl}$*FoxP3*^{Cre} (Stat3$^{fl/fl}$ + KO) mice were analyzed 10 days post-immunization with NP-OVA in CFA.

(D) Splenic T_{FR}, T_{FH}, GC B cells, and Bcl6+IL-17A^{+} in Treg.

(E) Frequency of T_{FR} and Bcl6^{+}IL-17A^{+} in Treg and in serum anti-NP IgG titers.

(F) FoxP3 expression in T_{FR} by the indicated mouse strains.

In (A)–(C), the data represent one of two experiments (C: n = 4/group). In (D)–(F), the results are pooled from two independent experiments (E, n = 4–9/group). *p < 0.05, **p < 0.01, ***p < 0.001, and ****p < 0.0001 (unpaired two-tailed Student's t test). Error bars indicate means ± SEMs.

See also Figure S5.

KEY RESOURCES TABLE

REAGENT or RESOURCE	SOURCE	IDENTIFIER
Antibodies		
Anti-mouse CD4 (GK1.5)	BD Biosciences	Cat# 552051; RRID: AB_394331
Anti-mouse CD4 (RM4–5)	Biolegend	Cat# 100531; 100559; RRID: AB_493374; RRID: AB_2562608
Anti-mouse TCRβ (H57–597)	Biolegend	Cat# 109220; RRID: AB_893624
Anti-mouse CD3 (145–2C11)	Biolegend	Cat# 100233; 100306; RRID: AB_2561387; RRID: AB_312671
Anti-mouse CD25 (PC61)	BD Biosciences	Cat# 553866; RRID: AB_395101
Anti-mouse CD25 (PC61)	Biolegend	Cat# 102025; RRID: AB_830744
Anti-mouse CD69 (H1.2F3)	Biolegend	Cat# 104512; RRID: AB_493564
Anti-mouse GITR (DTA-1)	Biolegend	Cat# 126308; 126317; RRID: AB_1089125; RRID: AB_2563385
Anti-mouse CTLA-4 (UC10–4B9)	Biolegend	Cat# 106306; RRID: AB_313255
Anti-mouse KLRG1 (2F1/KLRG1)	Biolegend	Cat# 138410; 138418; RRID: AB_10643582; RRID: AB_2563015
Anti-mouse Blimp1 (5E7)	BD Biosciences	Cat# 563643; RRID: AB_2738342
Anti-mouse TIGIT (1G9)	Biolegend	Cat# 142103; RRID: AB_10895760
Anti-mouse RORγt (B2D)	eBioscience	Cat# 12698182; RRID: AB_10807092
Anti-mouse CCR6 (29–2L17)	Biolegend	Cat# 129807; RRID: AB_1227498
Anti-mouse ST2 (RMST2–2)	eBioscience	Cat# 46933580; RRID: AB_2573882
Anti-mouse ST2 (DIH9)	Biolegend	Cat# 145303; RRID: AB_2561914
Anti-mouse Granzyme B (NGZB)	eBioscience	Cat# 11889882; RRID: AB_10733414
Anti-mouse Granzyme B (GB11)	Biolegend	Cat# 515408; RRID: AB_2562196
Anti-mouse IL-23R (12B2B64)	Biolegend	Cat# 150903; RRID: AB_2572188
Anti-mouse Bcl2 (3F11)	BD Biosciences	Cat# 554221; RRID: AB_395312
Anti-mouse Bim (C34C5)	Cell Signaling Technology	Cat# 12186; RRID: AB_2797842
Anti-mouse Helios (22F6)	Biolegend	Cat# 137229; 137220; RRID: AB_2561639; RRID: AB_10690535
Anti-mouse Ki-67 (SolA15)	eBioscience	Cat# 12569882; RRID: AB_11150954
Anti-mouse CD138 (281–2)	BD Biosciences	Cat# 553713; RRID: AB_394999
Anti-mouse CD45.1 (A20)	Biolegend	Cat# 110728; RRID: AB_893346
Anti-mouse CD45.2 (104)	Biolegend	Cat# 109837; RRID: AB_2561393
Anti-mouse CD19 (1D3)	BD Biosciences	Cat# 551001; RRID: AB_394004
Anti-mouse B220 (RA3–6B2)	BD Biosciences	Cat# 553090; RRID: AB_394620
Anti-mouse B220 (RA3–6B2)	eBioscience	Cat# 25045282; RRID: AB_469627
Anti-mouse CD44 (IM7)	Biolegend	Cat# 103028; RRID: AB_830785
Anti-mouse CD62L (MEL-14)	Biolegend	Cat# 104441; RRID: AB_2561537
Anti-mouse Fas (15A7)	BD Biosciences	Cat# 554258; RRID: AB_395330
Anti-mouse IgM (II/41)	eBioscience	Cat# 11579081; RRID: AB_465244
Anti-mouse T-/ B cell activation Ag (GL7)	Biolegend	Cat# 144606; RRID: AB_2562185

REAGENT or RESOURCE	SOURCE	IDENTIFIER
Anti-mouse ICOS (C398.4A)	Biolegend	Cat# 313508; 313518; RRID: AB_416332; RRID: AB_10641280
Anti-mouse PD-1 (J43)	BD Biosciences	Cat# 551892; RRID: AB_394284
Anti-mouse PD-1 (29F.1A12)	Biolegend	Cat# 135216; 135213; RRID: AB_10689635; RRID: AB_10689633
Anti-mouse IFN-γ (XMG1.2)	BD Biosciences	Cat# 554412; RRID: AB_395376
Anti-mouse IL-10 (JES5–16E3)	BD Biosciences	Cat# 554467; RRID: AB_395412
Anti-mouse IL-4 (11B11)	Biolegend	Cat# 504112; RRID: AB_493323
Anti-mouse IL-17A (eBio17B7)	eBioscience	Cat# 50717782; RRID: AB_11220280
Anti-Human/mouse Bcl6 (K112–91)	BD Biosciences	Cat# 561522; RRID: AB_10717126
Anti-mouse FoxP3 (FJK-16 s)	eBioscience	Cat# 25577382; 45577382; RRID: AB_891552; RRID: AB_914351
Anti-mouse CXCR5 (2G8)	BD Biosciences	Cat# 551960; RRID: AB_394301
Streptavidin-APC	Biolegend	Cat# 405207
Streptavidin-APC.Cy7	Biolegend	Cat# 405208
Anti-mouse CD90.1 (OX-7)	Biolegend	Cat# 202535; RRID: AB_2562643
Anti-mouse NK1.1 Biotin (PK136)	Biolegend	Cat# 108704; RRID: AB_313391
Anti-mouse B220 Biotin (RA3–6B2)	Biolegend	Cat# 103204; RRID: AB_312989
Anti-mouse CD4 Biotin (GK1.5)	Biolegend	Cat# 100404; RRID: AB_312689
Anti-mouse CD8 Biotin (53–6.7)	Biolegend	Cat# 100704; RRID: AB_312743
Anti-Human/mouse pSTAT5 (47/Stat5, pY694)	BD Biosciences	Cat# 612599; RRID: AB_399882
Anti-Human/mouse pSTAT3 (4/P-STAT3, pY705)	BD Biosciences	Cat# 612569; RRID: AB_399860
Annexin-V	BD Biosciences	Cat# 561012; RRID: AB_2034024
Anti-human IgG Fc (HP6017)	Biolegend	Cat# 409319; RRID: AB_2563329
Goat anti-mouse IgG Fc HRP	Invitrogen	Cat# A16084; RRID: AB_2534758
Rat anti-mouse IgG1 (X56) HRP	BD Biosciences	Cat# 559626; RRID: AB_397292
Purified Anti-Mouse CD16/CD32 (Fc Block)	BD Biosciences	Cat# 553142; RRID: AB_394657
Purified NA/LE anti-mouse CD3 (145–2C11)	BD Biosciences	Cat# 553057; RRID: AB_394590
Purified NA/LE anti-mouse CD28 (37.51)	BD Biosciences	Cat# 553294; RRID: AB_394763
AffiniPure F(ab')$_2$ Fragment Goat anti-IgM	Jackson Immunoresearch	Cat# 115–006–020; RRID: AB_2338469
Purified anti-Blimp1 (3H2E8)	Santa Cruz Biotechnology	Cat# sc-66015; RRID: AB_1119615
Purified anti-acetylated H3 (rabbit polyclonal)	Millipore	Cat# 06–599; RRID: AB_2115283
Rabbit IgG, polyclonal – Isotype control	Abcam	Cat# ab-171870; RRID: AB_2687657
Purified anti-H3K27me3 (mouse monoclonal)	Abcam	Cat# ab-6002; RRID: AB_1977539
Mouse IgG isotype control	Thermo Fisher Scientific	Cat# 10400C; RRID: AB_2532980
Monoclonal anti-β-actin-Peroxidase (AC-15)	Sigma	Cat# A-3584; RRID: AB_2765165
Hamster anti-mouse CD3ε (eBio500A2)	eBioscience	Cat# 14–0033–85; RRID: AB_837129
Alexa Fluor 568 goat anti-hamster IgG	Thermo Fisher Scientific	Cat# A-21112; RRID: AB_2535761
Alexa Fluor 647 rat anti-mouse IgD (11–26c.2a)	BioLegend	Cat# 405708; RRID: AB_893528
Rabbit anti-mouse Ki67 (polyclonal)	Thermo Fisher Scientific	Cat# PA5–19462; RRID: AB_10981523
Alexa Fluor 488 goat anti-rabbit IgG	Thermo Fisher Scientific	Cat# A-11008; RRID: AB_143165

REAGENT or RESOURCE	SOURCE	IDENTIFIER
Chemicals, Peptides, and Recombinant Proteins		
TransIT-LT1	Mirus	Cat# MIR2300
Tamoxifen	Sigma	Cat# T5648
Sunflower seed Oil	Sigma	Cat# S5007
Anti-mouse CD4 microbeads	Miltenyi Biotec	Cat# 130–049–201; RRID: AB_2722753
Anti-mouse CD19 microbeads	Miltenyi Biotec	Cat# 130–052–201
Anti-biotin microbeads	Miltenyi Biotec	Cat# 130–090–485; RRID: AB_244365
CFA	Sigma	Cat# F5881
IFA	Sigma	Cat# F5506
Imject Alum	Thermo Fisher Scientific	Cat# 77161
NP_{16}-OVA (16 loading)	Biosearch Technologies	Cat# N-5051–100
NP_{23}-KLH (23 loading)	Biosearch Technologies	Cat# N-5060–25
NP_{23}-BSA (23 loading)	Biosearch Technologies	Cat# N-5050–10
NP_{4}-BSA (4 loading)	Biosearch Technologies	Cat# N-5050–10
rhIL-2	Peprotech	Cat# 200–02
Mouse IL-21R Fc Chimera Protein	R&D Systems	Cat# 596-MR-100
Leukocyte Activation cocktail	BD Biosciences	Cat# 550583
Formaldehyde (16%, w/v), Methanol-free	Pierce	Cat# 28906
Protein G Dynabeads	Thermo Fisher Scientific	Cat# 10003D
Bouin's solution	Sigma	Cat# HT10132
Critical Commercial Assays		
FoxP3 staining Buffer Set	eBioscience	Cat# 00552300
BD Cytofix/Cytoperm Solution kit	BD Biosciences	Cat# 554714
Anti-nuclear Antibodies (ANA) Elisa kit	Alpha Diagnostic	Cat# 5210
IgE OptEIA ELISA Set	BD Biosciences	Cat# 555248
RNeasy plus micro kit	QIAGEN	Cat# 74034
TaqMan RNA-to-CT™ 1-Step Kit	Thermo Fisher Scientific	Cat# 4392653
ChIP-IT® Express Enzymatic	Active Motif	Cat# 53009
Chromatin IP DNA Purification Kit	Active Motif	Cat# 58002
Deposited Data		
Microarray dataset	This paper	GEO: GSE101611
Experimental Models: Cell Lines		
293 T	ATCC	Cat# CRL-3216; RRID: CVCL_0063
Experimental Models: Organisms/Strains		
Mouse: B6: C57BL/6J	Jackson Laboratories	Jax:000664; RRID: IMSR_JAX: 000664
Mouse: *Prdm1*$^{fl/fl}$: B6.129-*Prdm1*^{tm1Clme}/J	Jackson Laboratories	Jax:008100; RRID: IMSR_JAX:008100
Mouse: *FoxP3*^{Cre}: B6.129(Cg)-*Foxp3*$^{tm4(YFP/cre)Ayr}$/J	Jackson Laboratories	Jax:016959; RRID: IMSR_JAX:016959
Mouse: iCre^{+}: B6.129-*Gt(ROSA)26Sor*$^{tm1(cre/ERT2)Tyj}$/J	Jackson Laboratories	Jax:008463; RRID: IMSR_JAX:008463

REAGENT or RESOURCE	SOURCE	IDENTIFIER
Mouse: *Bcl6*$^{fl/fl}$: B6.129S(FVB)-*Bcl6*$^{tm1.1Dent}$/J	Jackson Laboratories	Jax:023727; RRID: IMSR_JAX:023727
Mouse: *Stat3*$^{fl/fl}$: B6.129S1-*Stat3*^{tm1Xyfu}/J	Jackson Laboratories	Jax:016923; RRID: IMSR_JAX:016923
Mouse: *Tcrα*$^{-/-}$: B6.129S2-*Tcra*^{tm1Mom}/J	Jackson Laboratories	Jax:002116; RRID: IMSR_JAX:002116
Mouse: FoxP3-GFP: B6.Cg-*Foxp3*^{tm1Mal}/J	Jackson Laboratories	Jax:018628; RRID: IMSR_JAX:018628
Mouse: *Rag2*$^{-/-}$: B6.129S6-*Rag2*^{tm1Fwa} N12	Taconic	Model# RAGN12; RRID: IMSR_TAC:ragn12
Mouse: B6SJL: B6.SJL-*Ptprc*^{a}-BoyAiTac	Taconic	Model# 4007; RRID: IMSR_CMMR:PST4007
Oligonucleotides		
ChIP-PCR *Il23r* forward	Integrated DNA Technologies	CTTGGCAAACTTCCTTCCTATTAAC
ChIP-PCR *Il23r* reverse	Integrated DNA Technologies	AAACAGTGCTGACTACTT GGCAT
ChIP-PCR *Il2ra* forward	Integrated DNA Technologies	TCGGAGAGGGATTCGGTAGCTTGA
ChIP-PCR *Il2ra* reverse	Integrated DNA Technologies	TGATAGCCTGCTGCTCAGAACTGGG
ChIP-PCR *Il2raCtrl* forward	Integrated DNA Technologies	TTACAGCAGTGCCTCCCTTG
ChIP-PCR *Il2raCtrl* reverse	Integrated DNA Technologies	GGGAGTGAGTGGGGTTAGGA
ChIP-PCR *Cxcr5* forward	Integrated DNA Technologies	GGGCAGGAAGAACAGAGTAAG
ChIP-PCR *Cxcr5* reverse	Integrated DNA Technologies	CTGCTAACCACAGAGGAAGAC
ChIP-PCR *Ccr7* forward	Integrated DNA Technologies	CACTCAAGCCAAGACAGCTA
ChIP-PCR *Ccr7* reverse	Integrated DNA Technologies	GACTACTCAACCAGGGTGTTC
ChIP-PCR *Ctla4* forward	Integrated DNA Technologies	AATATGTTTCTCTGCGGGCACCA
ChIP-PCR *Ctla4* reverse	Integrated DNA Technologies	GCCTAAGTAAACCCCAGATCAGC
ChIP-PCR *FoxP3* forward	Integrated DNA Technologies	CACCCTACCTGGGCCTATCC
ChIP-PCR *FoxP3* reverse	Integrated DNA Technologies	GCTTCATCGGCAACAAGGAG
shRNA targeting sequence: *Il23r*	Integrated DNA Technologies	CCTACATAGATACCAAGTATA
TaqMan probe for *Bcl6*	Thermo Fisher Scientific	Mm00477633_m1
TaqMan probe for *Prdm1*	Thermo Fisher Scientific	Mm00476128_m1
TaqMan probe for *Rps18*	Thermo Fisher Scientific	Mm02601777_g1
Recombinant DNA		
RV-pMIG-STAT5^{CA}	Johnston et al., 2012	N/A
pLKO.3 Thy1.1	Benoist and Mathis Lab (Harvard Medical School)	RRID: Addgene_14749
PsPAX2	https://tronolab.epfl.ch	RRID: Addgene_12260
pCMV-VSV-G	Stewart et al., 2003	RRID: Addgene_8454

REAGENT or RESOURCE	SOURCE	IDENTIFIER
Software and Algorithms		
FlowJo	FlowJo, LLC	v. 10; RRID: SCR_008520
FACSDiva	BD Bioscience	RRID: SCR_001456
Prism 6	GraphPad	v. 6; RRID: SCR_002798
ImageJ	NIH	RRID: SCR_003070
DAVID Bioinformatics Resources	https://david.ncifcrf.gov	v. 6.8; RRID: SCR_001881
Ingenuity Pathway analysis (IPA)	QIAGEN	RRID: SCR_008653